

①

AD-A286 320

PENN STATE



Enhancement of Corrosion Resistance and Mechanical Properties of Light-Weight Metals Through the Use of Graded Nonequilibrium Microstructures

Prepared and Submitted by:

Barbara A. Shaw
Kelly Kennedy
Department of Engineering Science and Mechanics
The Pennsylvania State University

Submitted to:
Office of Naval Research
800 North Quincey Street
Arlington, VA 22217-5000



October 1994



94-35250



94 11 15 062

PENN STATE



**Enhancement of Corrosion Resistance and Mechanical Properties of
Light-Weight Metals Through the Use of Graded Nonequilibrium
Microstructures**

**Barbara A. Shaw
Kelly Kennedy
Department of Engineering Science and Mechanics
The Pennsylvania State University**

October 1994

LIBRARY
X
A-1

TABLE OF CONTENTS

	page
Abstract	1
Introduction	1
Background	3
Experimental Approach	6
Results and Discussion	10
Summary and Conclusions	17
References	18
Tables	20
Figures	31

Abstract

Designs for the future will place extreme demands on light-weight materials. In order to meet the challenges of the future it is vital that an emphasis be placed on tailor-making these materials to enhance specific properties. Through the use of rapid solidification processing advances have been made in our ability to engineer materials, but we have yet to be able to tailor-make a light-weight alloy with all of the characteristics we desire. A new approach to tailor-making alloys with the enhanced properties we desire is to use nonequilibrium alloying techniques such as sputter or high-rate vapor deposition to grade the structure and composition of an alloy during processing. Such alloys could be designed to take advantage of recent advances in enhancing both the mechanical properties and the corrosion resistance of Al and Mg. For conventional Al alloys, a combination of high strength and significantly enhanced corrosion resistance are mutually exclusive. In order to achieve high strengths, precipitates are necessary in the microstructure. On the other hand in order to exhibit good corrosion performance, a one phase structure is usually required (precipitates can establish microgalvanic cells which lead to accelerated corrosion of the precipitate or the alloy adjacent to the precipitate). Both of these properties could be combined in one material, however, if the structure and composition of the alloy were graded during nonequilibrium processing of the alloys. Work during the first year of this investigation has focused on an evaluation of the morphology and residual stresses present in sputter-deposited Al-Mo and Al-W alloys (both constant and graded compositions) and their influence on alloy corrosion resistance. Results from this investigation reveal that it is possible to produce graded alloys with significantly enhanced corrosion resistance. The level of enhancement is dependent upon the initial solute concentration in graded alloys and the morphology of the sputtered alloy. The most important factor governing corrosion resistance of the alloys is morphology of the deposit with the densest structures yielding the best corrosion performance.

Introduction

The use of light-weight metals, such as Al and Mg, in severe environments could be significantly expanded if material properties such as strength, modulus, toughness and corrosion resistance could be engineered to fit specific applications. While rapid solidification processing (rsp) and other nonequilibrium alloying methods have led to the production of metals with specific enhancements in properties we have yet to be able to tailor-make materials with all of the characteristics we desire. A new approach to engineering materials which will meet the demands

of future designs is to alter the structure and properties of the material as a function of section thickness during processing. Spatial control of materials' properties is not a new concept - surface hardening treatments and coatings have been used for many years to alter a material's surface properties. By gradually transitioning from one material to another, stress concentrations can be reduced and material properties can be spatially optimized. Interest in functionally graded materials (FGMs) has been steadily increasing for the past 10 years and, at present, the most common processing routes include: diffusion processes, spray deposition, liquid or vapor infiltration, and powder processing. This research focuses on a less commonly used method, physical vapor deposition, for producing graded Al and Mg alloys. The vapor deposition route not only provides a convenient means for producing graded materials, it also allows us to circumvent equilibrium solubility limits associated with the more common processing routes and; thus, produce alloys with significantly enhanced corrosion resistance.

Previous ONR-sponsored research¹⁻⁵ has shown that the localized corrosion resistance of aluminum can be dramatically enhanced through nonequilibrium alloying with elements such as W, Mo, and Ta. In order to maintain this dramatically enhanced corrosion resistance it is necessary for the transition metal solute to remain in solid solution with the aluminum; in other words it is necessary to have a one phase alloy. If present, the second phase particles act as nucleation sites for pitting corrosion of the aluminum. However in order to produce high strength Al alloys, precipitation of a second phase is necessary. Grading the structure of nonequilibrium Al-Mo and Al-W alloys presents a unique means for combining both strength and corrosion resistance in the same alloy -- properties which are mutually exclusive in conventional aluminum alloys. By heat treating a graded nonequilibrium Al-Mo or Al-W alloy in which the outside layers have solute concentrations on the order of 15 to 20 atomic percent and the inside layers have solute concentrations of 8 to 10 atomic percent it should be possible to produce an alloy which has a uniform distribution of fine precipitates for strength through most of the section and a surface that is single-phased and amorphous for corrosion resistance. *The primary goals of this research are to investigate the structure and properties of graded nonequilibrium Al and Mg alloys in order to gain a better understanding of the effects of solute grading on mechanical and corrosion characteristics of the alloys. An additional objective of the research is to gain experience in producing graded structures -- experience that could be used to tailor-make monolithic and composite materials with enhanced strength, corrosion, and wear resistance.* Research in the past year has concentrated on the morphology and residual stresses present in sputter-deposited Al-Mo and Al-W alloys (both constant and graded compositions) and their influence on alloy corrosion resistance.

Background

Nonequilibrium alloying for enhancing corrosion resistance

It is well known that transition metals such as Mo, Ta, and W enhance the corrosion resistance of stainless steels. These same passivity enhancing elements can also dramatically improve the localized corrosion resistance of Al, provided that they remain in solid solution in the alloy.¹⁻⁶ Alloying additions of transition metals such as Mo, Ta, W, and Cr are not typically used to enhance the corrosion resistance of Al because they exhibit very low solubility limits in Al, well below 1 atomic % (all references to % are in atomic %), and at these concentrations exert little influence on corrosion behavior. However, the amount of solute in solid solution can be increased, by several orders of magnitude, and corrosion performance significantly enhanced if the alloys are produced using a nonequilibrium alloying method such as sputter or physical vapor deposition.

Previously, the roles that Cr, Si, Zr, Nb, Mo, Zn, Mg, Ta, V, Cu, Ti, and Er nonequilibrium alloying additions play in altering the protective nature of Al passive films have been investigated.^{1-4, 6-13} These alloys have been produced by ion implantation,⁷⁻¹¹ melt spinning,¹³ vapor deposition,¹² and sputter deposition.¹⁻⁶ Cost and practicality preclude the use of the first two techniques for large scale production, so that only results obtained using the latter two techniques will be discussed. Figure 1 summarizes the anodic polarization results for the most promising "stainless aluminum" alloys in aerated 0.1M KCl at a pH of 8. This figure reveals that pure Al and 5086 Al spontaneously pit in this environment. The nonequilibrium addition of Zr, Cr, Ta, Mo or W to Al results in the formation of increasingly more protective passive films as attested to by the positive shifts observed in the breakdown potential, E_b . The most significant enhancements in the localized corrosion resistance of these thin film alloys were observed for the Al-Cr, Al-Ta, Al-Mo, and Al-W alloys. In the aerated 0.1M KCl environment the alloys exhibited average increases in E_b of 600 mVSCE, 750 mVSCE, 800 mVSCE, and 2600 mV for Al-4%Cr, Al-6%Ta, Al-8%Mo and Al-9%W, respectively. The 2600 mV shift in the breakdown potential for Al with the addition of W is extraordinary. This polarization behavior is comparable to that exhibited by the most corrosion resistant stainless steels and nickel-based alloys.

Bulk nonequilibrium aluminum alloys (250 mm wide by 1.6 mm thick by 1 m long) have been produced in England by the Royal Aerospace Establishment (RAE) using a high-rate physical vapor deposition process.¹⁵⁻¹⁸ These Al-Cr-Fe alloys exhibit significantly enhanced mechanical properties which can be attributed to their fine grain structure and uniform distribution of 3 to 5

nanometer precipitates. The corrosion performance of the RAE alloys, while better than that of commercial Al alloys, is not comparable with the improvements seen for the single phase Al-Cr, Al-Mo, Al-Ta or Al-W alloys as illustrated in Figure 2.

Microstructure and stability of nonequilibrium alloys

Examination of sputter deposited pure and alloyed Al with high resolution scanning electron microscopy (HSEM) and transmission electron microscopy (TEM) reveals a fine structure with grain sizes of hundreds of nanometers or less depending upon the solute element present and its concentration. The average grain size for the sputter deposited Al, Al-6 to 10 % Mo, Al-6% Ta alloys was 250, 120 and 100 nm, respectively. Much finer structures were noted for the Al-W alloys, where grain sizes ranged from tens of nanometers to amorphous structures. The TEM micrographs in Figure 3 show the difference in grain size for an Al-5%Mo and an Al-5%W alloy sputtered under the same conditions. Selected area electron diffraction patterns for high W concentration alloys, see Figure 4, reveal that amorphous alloys can be produced. Frankel⁶ has found that high concentrations of other transition metals also result in amorphous alloys. Graded compositions would offer the possibility of designing amorphous surfaces for alloys.

Glancing angle x-ray diffraction¹⁴ has been used to characterize each of the stainless aluminum alloys shortly after deposition and as a function of time over several years to determine their metallurgical stability. No evidence of intermetallic phase formation was found in any of the alloys. The structures appear to be stable at room temperature over time with no precipitation of a second phase occurring after more than 2 years of room-temperature storage.

Research into the thermal stability of Al-Mo and Al-W alloys with solute concentrations ranging from less than 10% to greater than 20 % has revealed that precipitation at elevated temperature occurs readily at the lower solute concentrations and is retarded at the higher solute concentrations.¹⁵ While this may seem counter-intuitive, it appears to be a result of the amorphous nature of the higher solute concentration alloys. Al-Mo and Al-W alloys with solute concentrations greater than approximately 14% were amorphous in the as-deposited condition and after heat-treatment at temperatures up to 500°C for 1 hour. On the other hand, at solute concentrations less than or equal to 11 %, precipitation readily occurred at temperatures as low as 400°C after 1 hour.

The microstructure of the RAE vapor deposited Al-Cr reveals a supersaturated solid solution containing most of the chromium in solid solution with a fine dispersion of a 3 to 5 nm iron-

chromium phase and a small amount of grain boundary Al₇Cr intermetallic. The structure is stable after prolonged annealing at temperatures up to 260 °C.

Nonequilibrium alloying for enhancing mechanical properties

The mechanical properties of the RAE vapor deposited nonequilibrium Al alloys have been investigated in detail.^{12, 16-19} Table 1 compares some of the mechanical properties of the RAE vapor deposited materials to conventional high strength aluminum alloys and advanced Al alloys produced using more traditional rapid solidification technology.

The room temperature tensile strength of the vapor deposited alloys results from a combination of solute hardening from the high supersaturation of Cr, precipitation hardening from the fine dispersion of iron precipitates, and grain size/dislocation hardening.^{12, 15-18} The 7091 alloy shown in Table 1 is a well known powder metallurgy (PM) alloy with tensile strengths of 539 to 582 MPa reported for extruded and rolled sheet, respectively. The vapor quenched alloys show significant improvements in tensile strength over both the PM alloy and 7075-T6 with only small reductions in ductility. For the Al-7.5%Cr-1.2%Fe alloy a 40 % increase was observed in the yield strength in comparison to either 7075 Al or PM 7091 alloy. The modulus was found to increase with increases in chromium content. An increase in the modulus of 3 GPa/Wt. % Cr was observed for alloys with Cr concentrations ranging from 3 to 5 weight percent - these values are 20 to 30 % higher than those reported for Al-Li alloys.¹²

After exposure at 300 °C for 1000 hours, the vapor quenched Al-7.5%Cr-1.2%Fe alloy retained 75% of its room temperature tensile strength. The excellent elevated temperature strength has been attributed to the homogeneous dispersion of fine metastable precipitates. Rapidly solidified powder alloys being developed for high-strength/high-temperature applications derive their strength from precipitates on the order of 100 nm in diameter. The precipitates in the vapor quenched materials are more than an order of magnitude smaller than the precipitates in the PM alloys and result in elevated temperature tensile strengths 150 MPa higher for temperatures up to 250 °C for the vapor quenched alloys. The creep strength was found to be double that of the heat-resistant Concorde material CM003 as a result of the excellent thermal stability of the vapor quenched materials.

The fatigue performance of vapor deposited Al-7.5%Cr-1.2%Fe alloy is presented in Figure 5. Also shown in this figure for comparison are fatigue data for 7091-T7E69. At 10⁶ cycles an

endurance strength of 250 MPa was determined for the vapor deposited alloys. This value is twice the design target value for advanced high strength aluminum alloys of 124 MPa.

Experience with the RAE alloys has revealed the mechanical properties of Al can be enhanced through the precipitation of an Al-Cr-Fe phase from alloys supersaturated with Cr. Experience with sputter deposited nonequilibrium Al alloys reveals that one-phase alloys supersaturated with transition metals such as Cr, Mo, Ta, and W have pitting corrosion resistances similar to stainless steels. While the combination of a strong, precipitation-hardened material and a corrosion resistant one-phase alloy is not possible with conventional alloy production methods, it should be possible with a functionally graded, nonequilibrium Al alloy. Heat-treatment of the graded alloy could be used to get a fine distribution of precipitates through most of the section while an amorphous alloy with enhanced corrosion resistance is maintained at the alloy surface.

Experimental Approach

Alloy Fabrication

The majority of the alloys evaluated in this investigation were fabricated at the Materials Research Laboratory (MRL) at the Pennsylvania State University using a DC magnetron co-sputter deposition system. Figures 6 and 7 show the deposition system. In this system, the substrate (oxidized and unoxidized Si single crystal wafers) is oriented vertically and the substrate is separated from the target by a distance of 10 inches. Base pressures for the system were in the 10^{-5} to 10^{-6} Torr range. Either 240 Watts or 120 Watts of power was applied to the Al target and power to the solute was varied to produce the desired solute concentration. Immediately before placing the Si substrate on the substrate holder, the wafer was dusted-off with dry N₂ gas. In some cases the Si wafers were subjected to the cleaning procedure outlined below. Alloys produced on wafers cleaned according to this procedure are noted in Table 2 which lists all of the alloys evaluated in this investigation. During deposition, the substrate was rotated at 4.5 rpm to produce deposits with uniform solute concentration across the surface of the wafer. Alloy thicknesses ranged from 0.2mm to 0.7mm and the alloys reached temperatures of approximately 75°C during deposition.

Cleaning Procedure for Si Wafers

The cleaning procedure was a series of consecutive steps as follows:

Expose wafers to the following sequence of steps:

1. boiling de-ionized (DI) water for 5 minutes
2. hot isopropyl alcohol for 5 minutes
3. a solution containing 7 parts DI water, 2 parts hydrogen peroxide, and 1 part NH_4OH at a temperature between 75 and 85°C
4. a solution containing 7 parts DI water, 2 parts hydrogen peroxide, and 1 part HCl at a temperature between 75 and 85°C for 5 minutes
5. 5% HF solution for 1 minute
6. DI water for unlimited time
7. isopropyl alcohol for unlimited time
8. N_2 gas to dry

A limited number of alloys were produced at Martin Marietta Space Systems (MMSS) using a 602RS DC/RF Thin Film Deposition System which was custom built by Denton Vacuum. Details concerning this system and its operation have been presented elsewhere²⁰. In the MMSS system, the substrate is mounted horizontally and a distance of 10 cm separates the substrate and the targets. A power setting of 480 Watts was applied to the Al and, in the case of the graded alloys, the power to the solute targets was increased with time to produce the desired solute concentration profile. For both the MRL and MMSS alloys, the highest solute powers were used at the end of the deposition so that the highest solute concentration would be at the outside of the deposit. The last section of Table 2 lists pertinent characteristics for each of the alloys prepared at MMSS.

Compositional Analysis

All of the constant solute alloys fabricated at MRL were compositionally analyzed using direct current plasma spectroscopy (DCP). The initial and final compositions of the graded specimens were estimated based on the concentrations of the constant solute alloys fabricated at the same

power settings. Most of the films fabricated at MMSS were analyzed using energy dispersive spectroscopy (EDS) and a computer program (Tracor Northern Semi-Quantitative SQ software) to yield semi-quantitative compositional information. Compositions for all of the alloys (in atomic %) are given in Table 2.

Composition versus depth information for selected alloys was estimated with Auger electron spectroscopy (AES). AES was conducted at ALCOA Technical Center using a Physical Electronics Model 670 scanning Auger microprobe. In addition, an AES analysis was conducted on films prior to depth profiling to identify elements in the native oxide film. AES was conducted using an un rastered electron beam approximately 800Å in diameter. The sputtering rate for an Al₂O₃ barrier oxide standard was determined to be approximately 140Å/min and Auger data were collected every 0.25 or 0.5 minutes between sputtering intervals.

Alloy Characterization

Film thicknesses were determined using a Tencor Instruments Alpha-Step 200 profilometer and are listed in Table 2. When perfectly calibrated the measurement error with this instrument is 5Å. The thicknesses listed in Table 2 were determined by averaging the heights measured at three different points.

X-ray diffraction (XRD), using a Scintag PADV diffractometer, was conducted on each of the specimens to determine crystal structure of the alloys. Each specimen was scanned from 10° to 110° at a rate of 1 deg/min and, unless otherwise stated, the x-ray beam was at normal incidence to the specimen. A copper x-ray source was used and x-rays were collected by a Li drifted Ge detector at 45kV and 40 mA.

As-deposited and polarized film morphologies were characterized using optical microscopy, scanning electron microscopy (SEM), high resolution scanning electron microscopy (HSEM), or a scanning laser microscopy (SLM). Optical microscopy was performed using a Cambridge Instruments StereoZoom 7 microscope with variable magnifications from 10X to 70X. A Lasertec SLM Model 1LM11 was used for characterization at intermediate magnifications (245X to 4635X). Low-resolution scanning electron microscopy utilized an ISI Model SX40 microscope and high-resolution SEM utilized an ISI dual stage Model 130. Each as-deposited specimen was carefully examined using these microscopies to identify surface anomalies and defects. Electrochemically

tested specimens were also examined using SEM to characterize the morphology of breakdown sites (pits).

Intrinsic Stress Measurements

Intrinsic stresses in the alloys were determined by measuring the radius of curvature of thin (0.005 inch thick) polycarbonate sheets before and after deposition of the alloys. A schematic of the measurement method is presented in Figure 8. The system employs a modified He-Ne laser beam which is split into sections and reflected off the uncoated or alloy coated polycarbonate sheet. The radius of curvature is calculated by noting the differences in beam location with and without the alloy coating. Stoney's equation is then used to determine the residual stress. Note that since Stoney's equation is independent of the elastic modulus of the film an experimental error of 5 to 10 % can result ²¹.

Electrochemical Experiments

In order evaluate the corrosion resistance of the alloys anodic potentiodynamic polarization scans were generated on each of the alloys using either an EG&G Princeton Applied Research (PAR) Model 273 Potentiostat interfaced with a PC computer controlled by PAR Model 352 software, or a Gamry PC3 potentiostat controlled by CMS100 software. Tests were performed at room temperature using a quiescent 0.1MNaCl solution adjusted to pH 8 with NaOH. In this context the term quiescent is used to describe a solution which is open to the atmosphere and is not intentionally aerated or deaerated. The majority of the scans were generated at a rate of 0.2 mV/sec; however, a few experiments were conducted at a slower scan rate of 0.05 mV/sec to confirm breakdown potentials. Electrochemical specimens were prepared by attaching a lead wire and painting the backs and edges of cleaved sections of the wafer with a marine epoxy (Interlux 404/414) to isolate the electrical connection and expose only the alloy surface.

Results and Discussion

Compositional Analysis

Auger electron spectroscopy (AES) was used to estimate the solute concentration as a function of film thickness for the graded alloys. While this method will not give exact concentrations, it is useful in estimating compositional changes across the film and any differences between the estimated value obtained using Auger and the actual value should be constant. In future studies, it is hoped that Rutherford backscattering can be used to determine the exact solute gradients in the films. AES depth profiles for ungraded and graded Al-Mo alloys are presented in Figures 9 and 10. Analysis of these profiles revealed that the outer $\sim 100\text{\AA}$ of material analyzed corresponded to the passive oxide film on the alloy. This oxide layer is apparent because of the large initial oxygen concentrations and the small initial Al concentrations. The film/substrate interface for these alloys is approximately at the point where the Si concentration is 50% of its maximum. The Al alloy film is located between the oxide and the Si interface. Figure 9 clearly shows a constant solute concentration as a function of alloy thickness; whereas, Figure 10 shows a slight gradient in the alloy film with the highest solute concentration at the outer surface of the deposit. The composition gradient in the Al-Mo film is linear and is a result of linearly increasing the power to the solute target during deposition. The AES sputter profiles for some of the alloys showed an Al_2O_3 peak at the film/substrate interface and oxygen within the sputtered films as illustrated in Figures 11-13. This peak at the film-substrate interface and the presence of oxygen in the film are the result of an air leak into the vacuum system at one point in time.

AES of the surface was also conducted on each of the alloys that were depth profiled. Results showed that no Mo was present in the oxide of the Al-Mo films, and that some W was present in the initial oxide layer for the Al-W alloys (with the exception of Al - ~ 3 to 7% W alloy, where no W was observed in the initial oxide layer). Other elements found on the surface of the passive film were C, Al, O, and S (in some cases).

Alloy Characterization

X-Ray Diffraction

X-ray diffraction analysis of the alloys produced at the MRL revealed that all of the Al and Al-Mo films, both graded and constant, were crystalline; whereas, all but the lowest W concentration alloy examined were amorphous. No evidence of Al-Mo or Al-W precipitates was found. In the past

, we found that crystallinity was a function of solute concentration and/or deposition temperatures. In this previous work, amorphous Al-W alloys were noted at solute concentrations as low as 8% when a liquid nitrogen cold stage was used. The present work suggest that deposition conditions (inherent to the particular deposition system) may also influence film crystallinity since amorphous alloy were noted at W concentration as low as 7% in this work.

As-Deposited Alloy Morphology

Almost all of the as-deposited alloy films contained some surface anomalies or defects. Defects are not uncommon in sputter films and can be present in one or several forms within any given film. Depending on the nature of these anomalies, they may act as the nucleation sites for early breakdown/pitting of the alloy (and account for the significant variations sometimes observed in the breakdown potentials for specimens taken from different areas of the same alloy film) or they may have no effect on corrosion performance at all. In addition, it has been reported that film defects may cause a redistribution of stress in the alloy²².

Figure 14 [Al - (0 to 14%)W graded alloy], Figure 15 [Al - 5%Mo constant solute alloy], and Figure 16 [Al - 3%Mo constant solute alloy] all show surface protrusions on as-deposited alloys, possibly resulting from dust particles on the substrate surface prior to alloy deposition. Note that in Figures 14 and 15 cracks can be seen in the deposited film. Figure 16 shows a protrusion and, in this case, no cracking was observed. An analysis of the intrinsic stress, which will be presented in the next section, will show that the films in Figures 14 and 15 are in tension, whereas, the film in Figure 16 is in compression. Tensile films are commonly defined as "too few atoms per selected area" and compressed films are defined as "too many atoms per selected area". A possible explanation for the differences seen in these micrographs is that the residual tensile stress in the films pictured in Figures 14 and 15 resulted in cracking of the alloy over the dust particle; whereas, the residual compressive stress in the film pictured in Figure 16 kept a crack from opening up over the dust particle. It is anticipated that electrochemical test specimens that contain protrusions with cracks (residual tensile stress in the film) will show degraded corrosion performance in comparison to specimens that contain protrusions without cracks (residual compressive stress).

Figure 17 [sputter deposited pure Al], Figure 18 [Al - 6.5%Ta constant solute alloy], and Figure 19 [Al - 10%W] all show large indentations in the surface of the alloy. These "holes" probably were not deep enough to expose the substrate, but they may expose underlying layers of lower solute concentrations in the graded alloys. Like the cracks at surface protrusions, these indents

may act as nucleation areas for breakdown (depending on their geometry and whether or not the Si substrate is exposed).

Figures 20 - 23 display various forms of scratches observed on the as-deposited alloy films. Figures 20 and 21 show irregular scratches on graded Al-W alloys (with the W concentration varying from 0% near the substrate to 14 % at the surface). Figure 22 shows a scratch on a cleaved, uncleaned silicon substrate. Scratches in the substrate such as this one have been observed to translate through the deposited film and be visible on freshly deposited alloy surfaces. Figure 23 shows a scratch and a circular discolored region on an Al - 6.5%Ta constant solute alloy. Scratches can also result from the cleaving process used to prepare our electrochemical specimens. Again depending on their nature, these scratches could act as nucleation sites for pitting.

Figures 24 through 28 display various surface morphologies observed for sputter deposited pure Al films. Figures 24 through 26 are HSEM micrographs of pure Al sputtered at MRL, MMSS, and Martin Marietta Laboratories (MML), respectively. Deposition conditions at MML varied from the others in that specimens were fabricated in a class 100 clean room and the deposition was conducted on a substrate placed on a liquid nitrogen cold stage. Note that these micrographs are all at the same magnification. The bright spots in the photos show higher regions on the film. Thus, the MRL film had the highest amount of overall surface roughness, but no large areas with concentrated growth. On the other hand, the MML aluminum film was relatively smooth overall, but had a few areas of concentrated growth. Overall the MMSS alloy film was very smooth, but again, a few areas of concentrated growth were observed. Figures 27 and 28 are higher resolution micrographs of the MML and MMSS Al films showing areas of concentrated growth. The large grains observed in the MMSS film, Figure 27, are believed to be hillocks. Hillocks are commonly seen in Al thin films under conditions of high compressive stress.²² Mechanisms for hillock growth are still under investigation, but one study suggested that the compressive stresses were relaxed by the diffusion of the material from the bulk of the film to the surface²². No explanation could be found for the "cauliflower-type" structures, pictured in Figure 28, which were observed on the MML Al films.

Intrinsic Stress Measurements

A graph of residual stress versus solute concentration for Al-W alloys deposited at an Al target power setting of 120 Watts is presented in Figure 29. As W is added to the Al, an initial increase in the compressive stress was noted. At a W concentration of 10.8% a tensile stress of 0.145

GPa was observed and the stress in the deposit remained tensile as the W concentration increased. By cross-sectioning the thin-film alloys and examining the morphology of the deposit (using HSEM) it is also possible to gain information concerning the type of residual stress (tensile or compressive) present in the film.

Cross-sectional microstructures of the alloys examined in Figure 29 are displayed in Figure 30. The Al-6.4%W shows a very dense, compact microstructure that is characteristic of a highly compressed film. Microstructures of the higher solute concentration alloys (Al-14.6%W, Al-16.4%W, and Al-37%W) were found to be quite different than that of the compressed Al-6.4%W alloy. Fine columnar growth is apparent in the microstructures of these higher solute concentration alloys -- indicating tensile stress in the film and confirming the residual stress measurements. The roughness observed in the cross section of Al-14.6W may be a result of oxygen in the film. Auger analysis was not conducted on this specimen, but another source indicates that this "multiply fractured cross section" results from the presence of oxygen throughout the film thickness.²³ The surface morphologies of the Al-16.4%W and Al-37%W alloys revealed that the individual columns had pointed tops.

A graph of residual stress versus alloy composition for Al-W alloys with 6.6, 7, 21.7, and 24.1 % W deposited at an Al target power setting of 240 Watts is presented in Figure 31. This graph shows that as W is added to Al, the stress in the film changes from compression to tension. At a solute concentration of 6.7% a residual tensile stress was measured; whereas, a compressive stress was measured at a slightly higher solute concentration of 7%W. Perhaps more data points at these concentrations would reveal that the data point at 7% is in error or that the average of the two is actually closer to the real stress at these solute concentrations. At a solute concentration of 21.7%, a residual tensile stress of 0.1 GPa was measured which appears to switch to a compressive stress at the highest W concentration evaluated (24.1 %).

Cross-sectional microstructures of the alloys evaluated in Figure 31 are displayed in Figure 32. Pure aluminum shows a compressed, relatively dense cross-sectional microstructure with no distinct columnar growth. This observation is in agreement with the compressive residual stress measured for pure Al. The topography of the surface for pure Al was found to be rough as the earlier SEM characterization of the surface revealed. The smooth surface on the left side of the pure Al micrograph is the underside of the film. Observation of the underside of the film reveals that initial film growth is smooth and that roughness becomes apparent as the film grows. The alloys with 6.6 and 7 % W exhibited very similar microstructures with distinct columnar growth which is characteristic of tensile stress in the film. This observation casts doubt on the

compressive residual stress measurement for the Al-7%W film. Additionally, both alloys have a rough surface morphology. Finally, the Al-22%W, which is in a higher tensile state than the 6.6%W alloy, shows a significant difference in film microstructure and topography when compared to the lower solute concentration alloy. This sample also shows columnar grain growth, but the grains are now significantly thinner and more dense. The surface morphology of this alloy indicates that the tip of each column forms a point. In contrast to these cross-sections, the cross-sections for the Al-W alloys produced at an Al target power setting of 120 Watts revealed much denser and smoother films.

A graph of residual stress versus solute concentration for Al-Mo alloys with Mo concentrations up to 10.5 % is presented in Figure 33. At a Mo concentration of 3.4% Mo, a compressive residual stress was measured. When the Mo concentration was increased to 5.5 %, a tensile stress was measured. Finally, at the higher Mo concentrations (9 and 10.5%) the stress was, again, found to be compressive.

Cross-sectional microstructures of the alloys examined in Figure 33 are presented in Figure 34. The microstructure of pure Al was shown in Figure 32 and it exhibited a compressive stress with no distinct columnar structure. The Al-3.4%Mo alloy microstructure also exhibited a compressive stress with some columnar growth apparent in the upper half of the film. Additionally, the tips of each column were pointed. The lower portion of this film appears to be in compression with very little columnar growth detected. The next micrograph, Al-5%Mo, exhibited a relatively low tensile stress. The tensile stress in the film is reflected by the distinct columnar growth and large grain diameters seen throughout the film profile. Furthermore, the tips of each column are pointed. The Al-9%Mo alloy exhibited a compressive stress and showed a dense, compact cross-section with no distinct columnar growth. These microstructures confirm the type of residual stress present at each point in the graph shown in Figure 33. The Al-3.4 to 9%Mo alloy shown in this figure will be discussed in the following paragraph.

The results presented above clearly show that the residual stress and microstructure change as the solute concentration in the alloy changes. Thus, stress and microstructural gradients are expected to appear throughout the thickness of a compositionally graded alloy. The graded Al-3.4 to 9%Mo alloy shown in Figure 34 exhibits microstructural changes as a function of alloy depth. From the stress versus solute concentration graph shown in Figure 33, it is expected that the initial deposit will have a compressive stress and a morphology similar to that of the Al-3.4%Mo alloy. This compressive stress is identified by the lack of columnar growth in the initial layers of the deposit. With continuing deposition, and an increase in solute concentration, the stress in the deposit are

expected to change in the same manner as that illustrated in Figure 35. Thus, the distinct columns seen in the mid-region of the microstructure reflect the tensile stresses that become apparent as the solute concentration increases. Finally at the highest solute concentrations, the stress versus composition graph indicates that the alloy will become compressive again. The increase in column width and rounding of the ends of the columns in the microstructure at the surface of the film appears to correspond to the change in stress at high solute concentrations. Similar morphology variations have been noted in cross-sections of other graded Al-Mo and Al-W alloys.

Corrosion Resistance

Anodic potentiodynamic polarization was conducted on all of the alloys to evaluate corrosion resistance and the results of these experiments are summarized in Table 3. This table reveals that both the corrosion potential and the breakdown (pitting) potential increase as the solute concentration increases - for both the constant composition and graded alloys. In addition, it should be noted that the breakdown potentials for the graded alloys were slightly less than that of the constant solute alloys having the same solute concentration as the graded alloy's outer layer. Duplicate, and in some cases triplicate, polarization scans were conducted on every alloy to assess reproducibility of the corrosion behavior. Variations in the breakdown potentials for a given alloy are believed to be the result of surface anomalies/defects and the statistical nature of the pitting process. In addition, holes or scratches at the surface of the graded alloys may expose underlying layers with lower solute concentrations resulting in breakdown at lower than expected potentials. The higher breakdown potentials noted for a couple of the pure Al specimens was the result of oxygen in the deposited film and is not indicative of the true breakdown potential for pure aluminum which is typically in the range of -680 to -710 mV_{SCE} in 0.1M NaCl. Figures 35 through 37 show polarization scans with typical, good, and very poor reproducibility, respectively.

Anodic polarization scans for Al-Mo and Al-W alloys (both constant and graded compositions) are presented in Figures 38-43. Again, the compositionally graded alloys have the highest solute concentrations on the outer layers of the alloy and lowest solute concentrations at the alloy/substrate interface. Polarization behavior for pure Al has been included in these figures for comparison. These figures show that the graded alloys exhibit behavior similar to the highest constant solute concentration alloys and that the breakdown potentials are generally closest for the alloys with the highest initial solute concentrations. This difference in corrosion performance with initial solute concentration in the graded alloys is believed to result from exposure of underlying

layers of lower solute concentration through defects or pores in the film -- the higher the solute concentration at the base of these defects (the shallower the solute gradient) the more similar the corrosion resistance is to the constant solute alloys. The sputtered films produced at MRL are also much thinner than the alloys produced in some of our other programs. Note that in all cases, the breakdown potentials for the alloys are significantly higher than that of pure Al (or any commercial Al alloy). In Figure 43, the poor performance of the alloy is believed to be due to defects or pores in the alloy exposing interior regions of the deposit which have very low solute concentrations.

Figure 44 shows anodic polarization behavior for selected constant solute concentration Al-W alloys as a function of deposition conditions (either 240 or 120 Watts of power to the Al target). This figure reveals that deposit morphology appears to play a more important role than either solute concentration or stress state in the film in determining alloy corrosion resistance. The breakdown potential for an Al-5.9 %W alloy deposited at an Al power setting of 120 Watts (where the films exhibited a dense morphology) was almost equivalent to the breakdown potential obtained for an Al-21.7% W alloy deposited at an Al power setting of 240 watts (where the films had a more open morphology).

SEM micrographs of breakdown sites (pits) on an Al-5% Mo specimen after anodic polarization in 0.1M NaCl, revealing selective dissolution of Al in the pits, are presented in Figures 45 and 46. Figure 45 shows a large portion of a pit with the majority of the pit cover still present and Figure 46 shows a higher magnification image of small pits adjacent to the large pit. The numbers on these micrographs correspond to sites where EDS was conducted. Table 4 lists Mo:Al ratios for the various points identified in the micrographs. Points 1 and 9 represent the unattacked sputter-deposited alloy and show the lowest Mo:Al ratio. Points 2 and 4 were taken on the pit cover and show also show low Mo:Al ratios. Points 4,5,6,7 showed high Mo:Al ratios and represent either a small region of corroded alloy still remaining in the pit (point 3) or smaller breakdown sites where the corroded alloy and/or the corrosion product is still present in the pit. These solute enhanced regions have been observed in conjunction with Al-Mo pits in the past², but these micrographs confirm that the significant Mo enrichment is not in the passive film -- instead it appears to be in the alloy remaining in the pit.

Summary and Conclusions

The research during the first year of this program has shown that it is possible produce compositionally and structurally graded nonequilibrium Al-Mo and Al-W alloys with significantly enhanced corrosion resistance. This corrosion resistance is far superior to that of Al, and commercial aluminum alloys, and can even approach that of the constant solute alloys. Based on this research, the following conclusions can be drawn:

1. Sputter deposited thin-film alloys usually contain inherent defects, such as hillocks, cracks, and scratches, which may act as nucleation sites for pitting.
2. Residual stresses in sputter-deposited nonequilibrium Al-Mo and Al-W alloys are dependent on the solute concentration of the alloy. The type of stress present in the film (tensile or compressive) can be identified in the cross-sectional microstructure. Tensile films show columnar growth with boundaries visible between the individual columns. Depending on the Al power level and the amount of solute present, tensile cross-sectional morphologies vary from somewhat open structures with some voids visible (higher Al power setting or lower solute concentration) to very dense packing of the columns with no voids (lower Al target power setting or higher solute concentration). Compressive stress in the film results in a dense cross-section that appears glassy with little discernible structure at a magnification of 20,000X.
3. The primary factor governing corrosion resistance of the nonequilibrium alloys appears to be morphology of the deposit, with dense films (either tensile or compressive) exhibiting the best performance.
4. The compositionally graded Al-Mo and Al-W exhibit significantly higher breakdown potentials in a chloride environment than pure aluminum (or any commercial Al alloy) and when the initial solute concentration in the graded alloys is not too low, these alloys perform almost as well as constant solute concentration alloys.

ACKNOWLEDGMENTS

Special thanks to S. B. Krupanidhi and Ed Principe for their help with deposition of the alloys and to Brian Strohmeier at Alcoa Technical Center for conducting the Auger analysis.

References

1. W.C. Moshier, G.D. Davis, J.S. Ahearn, and H.F. Hough, *J. Electrochem. Soc.* 133, 1063 (1986).
2. W.C. Moshier, G.D. Davis, J.S. Ahearn, and H.F. Hough, *J. Electrochem. Soc.* 134, 2677 (1987).
3. W.C. Moshier, G.D. Davis, and G.O. Cote, *J. Electrochem. Soc.* 136, 356 (1989).
4. G.D. Davis, W.C. Moshier, T.L. Fritz, and G.O. Cote, *J. Electrochem. Soc.*, 137, 422 (1990).
5. B.A. Shaw, T.L. Fritz, G.D. Davis, and W.C. Moshier, *J. Electrochem. Soc.*, 137, 1317 (1990).
6. G.S. Frankel, M.A. Russak, C.V. Jahnes, M.Mirzamaani, and V.A. Bruslic, *J. Electrochem. Soc.*, 136, 1243 (1989).
7. A.H. Al-Saffar, V. Ashworth, A.K.O. Vairamov, D.J. Chivers, W.A. Grant, R.P.M. Procter, *Corr. Sci.*, 20 127 (1980).
8. M.V. Zeller and J.A. Kargol, *Appl. Surf. Sci.*, 18, 63 (1984).
9. P.M. Natishan, E. McCafferty, and G.K. Hubler, *J. Electrochem. Soc.*, 133, 1061 (1986).
10. E. McCafferty, G.K. Hubler, P.M. Natishan, P.G. Moore, R.A. Kant, and B.D. Sartwell, *Mater. Sci. Engr.*, 86, 1 (1987).
11. P.M. Natishan, E. McCafferty, and G.K. Hubler, *J. Electrochem. Soc.*, 135, 321 (1988).
12. R.W. Gardiner and M.C. McConnell, *Metals Matl.* 3, 254 (1987)
13. M. Fass, D. Itzhak, D. Eliezer, F.H. Froes, *J. Mater. Sci. Lett.*, 6, 1227 (1987).
14. B. A. Shaw, G.D. Davis, T.L. Fritz, B.J. Rees and W.C. Moshier, *J. Electrochem. Soc.*, 138, 3288 (1991).
15. R.G. Wendt, W.C. Moshier, B.A. Shaw, and P.L. Miller, *Corrosion*, 50, 820 (1994).
16. R.L. Bickerdike, D. Clark, J.N. Easterbrook, G. Hughes, W.N. Mair, P.G. Partridge, and H.C. Hanson, *International Rapid Solidification*, 1, 305 (1985).
17. R.L. Bickerdike, D. Clark, J.N. Easterbrook, G. Hughes, W.N. Mair, P.G. Partridge, and H.C. Hanson, *International Rapid Solidification*, 2, 1 (1986).
18. P.G. Partridge and M.C. McConnell, *Acta Metall.*, 35, 1973 (1987).
19. P.G. Partridge and M.C. McConnell, *Acta Metall.*, 35, 1981 (1987).
20. B.A. Shaw, T.R. Schrecengost, W.C. Moshier, and R.G. Wendt, *Inhibiting Corrosion in Gr/Al and Gr/Mg Metal Matrix Composites Using Nonequilibrium Alloying Techniques*, 1st Annual Report submitted to ONR June 1992.

- 21.[10.] Abner Brenner, Seymour Senderoff, "Calculations of Stress in Electrodeposits from the Curvature of a Plated Strip", Part of the Journal of Research of the National Bureau of Standards, Research Paper RP1954, vol.42, Feb.1949.
22. [6.] Kazakos, Fahnline, Messier, Pilione, "Compositional Dependence of Stresss inSilver Copper Alloys Prepared by Direct Current Magnetron Sputtering", J. Vac. Sci. Technol. A 10(6), Nov/Dec 1992, 3439-3444.
23. [11.] A.P. Thakoor, S.K. Khanna, R.M. Williams, R.F. Landel, "Influence of the Microstructure on the Corrosion Behavior of Magnetron Sputter-Quenched Amorphous Metallic Alloys", J. Vac. Sci. Technol.A, 1(2), Apr-June 1983, 520-523.

TABLE 1
Mechanical Properties of Vapor Deposited Alloys and Selected Al Alloys¹²

	TS	YS	% elong.	E	Fat. Strength**	Fract. Tough*** MPam ^{1/2}
	MPa	MPa		GPa	MPa	
7075-T6 (clad)	503	448	8	71		66
7075-T6	570	505			160	
7091-T7E69	539	505	9.5		125	
VD Al-7Cr-1.0 Fe		692	684	6.7	85	
VD Al-7.5Cr-1.2Fe		723	709	7.5	89	250 89.5
VDAl-8.6Cr-1.5Fe		818	808	5.0	92	

** constant amplitude fatigue tests on sheet specimens with a central hole, stress concentration factor of 2.5, L-T orientation***plane stress toughness

Table 2 Films Fabricated at MRL and MMSS

MRL Materials ⁴	Cleaned Si	Date Deposited	Deposition Time (min)	Atomic % Solute	Avg. Alloy Thickness	Avg. Alloy Stress (GPa) ¹	XRD ²	Avg. Atomic % Oxygen ³	Comments
Al									
Al120.Si.Ar	no	2/26/93	30		0.13375um		N/D	14	holes apparent in film; galvanic couple w/ Si
Al120.Si.Ar Al120.PC.Ar	yes	9/22/93	120		0.4195 um	-0.10178 C	N/D	N/D	cloudy, milky film (i.e. contaminated)
Al240.Si.Ar	no	5/27/93	45				c	N/D	Deposition pressure = 4.5mTorr
Al240.Si.Ar Al240.PC.Ar	yes	9/21/93	75		0.5503 um	-0.09505 C	N/D	N/D	cloudy, milky film (i.e. contaminated)
Al240.Si.Ar Al240.PC.Ar	yes	9/23/93	75		0.3653 um	-0.12505 C	N/D	N/D	cloudy, milky film (i.e. contaminated)
Al240.Si.Ar Al240.PC.Ar	yes	11/12/93	75			-0.09936 C	N/D	N/D	cloudy, milky film (i.e. contaminated)
Al-Mo									
Al240.Mo7.Si.Ar	yes	9/16/93	75	3.41			c	N/D	film appears cloudy
Al240.Mo7.Si.Ar Al240.Mo7.PC.Ar	yes	9/16/93	75	3.4 *	0.4950 um	-0.04566 C	N/D	N/D	
Al240.Mo11.Si.Ar	no	5/28/93	45	5.04	0.30475 um		c	N/D	
Al240.Mo11.Si.Ar Al240.Mo11.PC.Ar	yes	9/16/93	75	5.45	0.5502 um	0.05758 T	N/D	N/D	
Al240.Mo18.Si.Ar	yes	9/15/93	75	9.01			c	0	
Al240.Mo18.Si.Ar Al240.Mo18.PC.Ar	yes	9/16/93	75	9 *	0.5415 um	-0.08221 C	N/D	N/D	
Al240.Mo25.Si.Ar Al240.Mo25.PC.Ar	no	2/1/94	75	10.5	0.887 um	-0.07325 C	c	N/D	Gate valve opened to 2.5cm.

Table 2 (continued)

MRL Materials ⁴	Cleaned Si	Date Deposited	Deposition Time (min)	Atomic % Solute	Avg. Alloy Thickness	Avg. Alloy Stress (GPa) ¹	XRD ²	Avg. Atomic % Oxygen ³	Comments
Al-W									
Al240.W10.Si.Ar	no	6/26/93	45	3.96	0.373125 um		N/D	N/D	
Al240.W20.Si.Ar	no	6/26/93	45	6.61	0.451375 um		c	N/D	
Al240.W20.Si.Ar Al240.W20.PC.Ar	no	3/22/94	75	6.6 *	0.793 um	0.04194 T	N/D	N/D	Deposited film is slightly cloudy.
Al240.W16.Si.Ar	no	5/27/93	45	7 *			a	N/D	
Al240.W16.Si.Ar	yes	9/13/93	82	7.19			N/D	N/D	
Al240.W16.Si.Ar Al240.W16.PC.Ar	no	9/14/93	75	7 *	0.5660 um	-0.05027 C	N/D	N/D	
Al240.W50.Si.Ar Al240.W50.PC.Ar	no	3/21/94	75	21.74	0.857 um	0.10729 T	N/D	N/D	
Al240.W9.SiO2.Ar Al240.W9.PC.Ar	no	3/31/94	75	24.08	0.770 um	-0.10681 C	N/D	N/D	
GRADED FILMS									
Al-W									
Al120.W(0-16).Si.Ar	no	5/27/93	33	5.69 total (0 to 14) *	0.10275 um		a	4 (as-deposited) 5 (polarized)	deposition pressure = 4.5mTorr, assuming linear comp. grade, for every 0.00934um, Δ at% of W = 0.5173%
Al120.W(0-20).Si.Ar	no	5/27/93	48	9.95 total (0 to 13) *			a	11(as-deposited) 20 (polarized)	assuming thickness of 0.12um & linear comp. grade, for every 0.0075um, Δ atm% W = 0.62187%
Al120.W(13-27).Si.Ar Al120.W(13-27).PC.Ar	no	2/2/94	75	22.68 total	0.420 um	0.12267 T	a	N/D	
Al120.W(20-27).Si.Ar Al120.W(20-27).PC.Ar	no	2/2/94	75	17.42 total (13 to 16)*	0.445 um	0.16028 T	a	4	
Al240.W(9-16).Si.Ar Al240.W(9-16).PC.Ar	no	2/2/94	75		0.952 um	0.02123 T	N/D	23	

Table 2 (continued)

MRL Materials ⁴	Cleaned Si	Date Deposited	Deposition Time (min)	Atomic % Solute	Avg. Alloy Thickness	Avg. Alloy Stress (GPa) ¹	XRD ²	Avg. Atomic % Oxygen ³	Comments
Al-Mo									
Al240.Mo(3-11).Si.Ar Al240.Mo(3-11).PC.Ar	no	1/30/94	75	2.32 total (0 to 5) *	0.415 um	-0.04651 C	c	5	
Al240.Mo(0-18).Si.ArC2 Al240.Mo(0-18).PC.ArC2	N/D	11/19/93	75	6.63 total	0.472 um	0.01674 T	N/D	8	anne'er attached incorrectly; barrier betw. targets on lid; assuming lunar comp. grade & thickness of 0.54um, for every 0.0018um, $\Delta atm\% Mo = 0.0221\%$
Al240.Mo(7-18).Si.Ar Al240.Mo(7-18).PC.Ar	no	1/30/94	75	5.54 total (3.4 to 9) *	0.637 um	0.03385 T	c	14	
Al240.Mo(11-25).Si.Ar Al240.Mo(11-25).PC.Ar	no	1/31/94	75	6.54 total (5 to 10.5) *	0.617 um	0.02623 T	c	N/D	
Al240.Mo(20-25).Si.Ar Al240.Mo(20-25).PC.Ar	no	1/31/94	75	9.59 total	0.617 um	-0.06616 C	c	N/D	
MMSS Films									
		Date Deposited	Atomic % Solute						
Al480.Mo20.Si.Ar		11/3/93	10 (DCP)						
Al480.Mo40.Si.Ar		1/20/92	20 (predicted)						
Al - Mo graded			2. .018 (predicted)						
Al480.W20.Si.Ar		9/14/92	10 (EDS)						
Al - 26W		6/16/93	13 (DCP)						
Al480.W40.Si.Ar		1/21/93	24 (EDS)						

Notes:

1. C = compression, T = tension
 2. c = crystalline, a = amorphous, N/D = not determined
 3. Average oxygen content in the alloy, excluding the passive film, measured by AES, N/D = not determined.
 4. Poly-carbonate (PC) sheets are used only for stress measurements.
- * Composition is based on the average of alloys sputtered under identical conditions.

Table 3 Polarization Test Results (all tests were conducted in quiescent 0.1M NaCl with the pH adjusted to 8 with NaOH)

MRL Materials ¹	Date Deposited	Date Tested	Atomic Solute %	Scan mV/sec	Eb (mV)	Ecorr (mV)	ip (uA/cm ²)	Comments
Al240.Mo7.Si.Ar.1	9/16/93	11/10/94	3.41	0.2	-366	-668		Viewed under SLM prior to pol.
Al240.Mo7.Si.Ar.2	9/16/93	11/10/94	3.41	0.2	-349	-672	0.693	Viewed under SLM prior to pol.
Al240.Mo11.Si.Ar.1	5/28/93	6/1/93	5.04	0.2	-7	-642		
Al240.Mo11.Si.Ar.2	5/28/93	6/1/93	5.04	0.2	-19	-646	1.93	
Al240.Mo18.Si.Ar.1	9/15/93	11/8/93	9.01	0.2	127	-528	9.1	
Al240.Mo18.Si.Ar.2	9/15/93	11/8/93	9.01	0.2	151	-597	10.86	
Al240.Mo25.PC.Ar.1	2/1/94	2/9/94	10.5	0.2	40 & 430	-535	0.713 & 2.93	Two apparent passive regions (repassivation occurred)
Al240.Mo25.PC.Ar.2	2/1/94	2/9/94	10.5	0.2	52	-534	0.675	After pol, a black surface w/ many white scratches are seen.
Al240.Mo25.FC.Ar	2/1/94	2/21/94	10.5	0.05	50	-598	0.562	Film possibly deadhered towards the end of the scan before Eb occurred.
Al240.Mo25.Si.Ar								
Al120.W10.Si.Ar.1	6/26/93	7/7/93	6.63	0.2	278	-774		Initial scan stopped during pol in passive region. Same sample was repol. w/ Ecorr stabilizing 15 min.
Al120.W10.Si.Ar.2	6/26/93	7/8/93	6.63	0.2	-347	-811		Film delaminated during pol.
Al120.W20.PC.Ar	1/30/94	2/21/94	12.97	0.2	452	-697	0.767	
Al120.W20.Si.Ar.1								
Al120.W20.PC.Ar	1/30/94	2/21/94	12.97	0.2		-719	3.65	Sample sometime delaminated during pol.
Al120.W20.Si.Ar.2								
Al120.W16.Si.Ar.3	2/20/93	4/16/93	16.59	0.2	434	-735	1.16	
Al120.W16.Si.Ar.1	2/20/93	4/16/93	16.59	0.2	677	-729	1.16	
Al120.W27.Si.Ar.1	9/13/93	11/10/93	18.51	0.2	240	-677	0.63	Viewed under SLM before pol.
Al120.W27.Si.Ar.2	9/13/93	11/10/93	18.51	0.2	530	-633	0.63	Viewed under SLM before pol.
Al120.W50.PC.Ar	3/20/94	4/27/94	32.15	0.2	141 & 281	-608	0.968 & 3.16	Two passive regions, but visible breakdown site seen only at the higher Eb.
Al120.W50.Si.Ar.1								
Al120.W50.PC.Ar	3/20/94	4/27/94	32.15	0.2	1,125	-618	0.951	
Al120.W50.Si.Ar.2								

Table 3 (continued)

MRL Materials ¹	Date Deposited	Date Tested	Atomic Solute %	Scan mV/sec	E _b (mV)	E _{corr} (mV)	i _p (μA/cm ²)	Comments
Al120. W(0 to 16). Si. Ar.1	5/27/93	6/16/93	5.69 total (0 to 14) *	0.2	-586	-704	0.246	Deposition pressure = 4.5mTorr
Al120. W(0 to 16). Si. Ar.2	5/27/93	6/16/93	5.69 total (0 to 14) *	0.2	-509			Deposition pressure = 4.5mTorr. LP filter was not added. After pol., film stripped upon rinse.
Al120. W(0 to 20). Si. Ar	5/27/93	6/16/93	9.95 total (0 to 13) *	0.2	118	-640	0.849	
Al120. W(0 to 20). Si. Ar	5/27/93	6/16/93	9.95 total (0 to 13) *	0.2	147	-652	0.736	
Al120. W(13-27). PC. Ar Al120. W(13-27). Si. Ar.1	2/2/94	2/9/94	22.68 total	0.2	-35	-703	6.4	Lots of white specks seen near 2 opposite corners prior to pol. <i>Sample delaminated during Ecorr.</i>
Al120. W(13-27). PC. Ar Al120. W(13-27). Si. Ar.2	2/2/94	2/9/94	22.68 total	0.2	155	-637	0.729	After pol, black film w/ many white scratches seen on surface.
Al120. W(20-27). PC. Ar Al120. W(20-27). Si. Ar.1	2/2/94	2/10/94	17.42 total (13 to 16) *	0.2	384	-679	0.76	Film: delaminated during pol (at ~ 90 v).
Al120. W(20-27). PC. Ar Al120. W(20-27). Si. Ar.2	2/2/94	2/10/94	17.42 total (13 to 16) *	0.2	393	-652	0.634	Film delaminated during pol (at ~ 250v). After pol., breakdown sites are seen.
Al120. W(9-50). PC. Ar Al120. W(9-50). Si. Ar	3/25/94	5/26/94	(5 to 32) *	0.2	145	-629	0.562	
Al120. W(9-50). PC. Ar Al120. W(9-50). Si. Ar	3/25/94	5/26/94	(5 to 32) *	0.2	375	-630	0.631	
Al120. W(25-50). PC. Ar Al120. W(25-50). Si. Ar.1	3/26/94	4/27/94	(16 to 32) *	0.2	550	-647	0.794	
Al120. W(25-50). PC. Ar Al120. W(25-50). Si. Ar.2	3/26/94	4/27/94	(16 to 32) *	0.2	325	-593	~1.0	
Al120. W(30-50). PC. Ar Al120. W(30-50). PC. Ar.1	3/29/94	4/27/94	(20 to 32) *	0.2	790	-602	1	
Al120. W(30-50). PC. Ar Al120. W(30-50). PC. Ar.2	3/29/94	4/27/94	(20 to 32) *	0.2	600	-599	1	

Table 3 (continued)

MRL Materials ¹	Date Deposited	Date Tested	Atomic Solute %	Scan mV/sec	E _b (mV)	E _{corr} (mV)	i _p (μA/cm ²)	Comments
GRADED FILMS								
Al240.Mo(3-11).PC.Ar Al240.Mo(3-11).Si.Ar.1	1/30/94	1/31/94	2.32 total (0 to 5) *	0.2	-525	-694	~ 2.51	After pol., one breakdown site and uniform rust color are seen. Sample was not stopped immediately after breakdown & sample sat in DI water all day after breakdown.
Al240.Mo(3-11).PC.Ar Al240.Mo(3-11).Si.Ar.2	1/30/94	1/31/94	2.32 total (0 to 5) *	0.2	-60	-698	~ 5.62	After pol., no breakdown site and uniform color are seen. Sample sat in DI water all day after breakdown.
Al240.Mo(3-11).PC.Ar Al240.Mo(3-11).Si.Ar	1/30/94	2/21/94	2.32 total (0 to 5) *	0.05	-509	-738	~ 0.804	After pol. many scattered white spots are seen and breakdown site seen at edge.
Al240.Mo(0-18).PC.ArC2 Al240.Mo(0-18).Si.ArC2.1	11/19/93	12/15/93	6.63 total	0.2	-350	-655	~ 1.0	
Al240.Mo(0-18).PC.ArC2 Al240.Mo(0-18).Si.ArC2.2	11/19/93	12/15/93	6.63 total	0.2	-350	-660	1	
Al240.Mo(7-18).PC.Ar Al240.Mo(7-18).Si.Ar.1	1/30/94	1/31/94	5.54 total (3.4 to 9) *	0.2	-110	-651	~ 7.94	
Al240.Mo(7-18).PC.Ar Al240.Mo(7-18).Si.Ar.2	1/30/94	1/31/94	5.54 total (3.4 to 9) *	0.2	50	-572	~ 6.31	
Al240.Mo(11-25).PC.Ar Al240.Mo(11-25).Si.Ar.1	1/31/94	2/9/94	6.54 total (5 to 10.5) *	0.2	-134	-625	~ 3.62	After pol., film is greenish tint. Breakdown site seen, but may have not broken completely through.
Al240.Mo(11-25).PC.Ar Al240.Mo(11-25).Si.Ar.2	1/31/94	2/9/94	6.54 total (5 to 10.5) *	0.2	-170	-646	~ 8.63	After pol., film is greenish tint.
Al240.Mo(11-25).PC.Ar Al240.Mo(11-25).Si.Ar	1/31/94	2/21/94	6.54 total (5 to 10.5) *	0.05	-40	-564	1.26	Very few white spots seen prior to pol. After pol, breakdown site at edge and many small breakdown sites are seen on surface. Also, many white specks seen on surface.
Al240.Mo(20-25).PC.Ar Al240.Mo(20-25).Si.Ar.1	1/31/94	2/9/94	9.59% total	0.2	-80	-569	1.58	Film delaminated during pol.
Al240.Mo(20-25).PC.Ar Al240.Mo(20-25).Si.Ar.2	1/31/94	2/9/94	9.59% total	0.2	-20	-569	1.78	Film did not delaminate during pol., but breakdown may have occurred by delamination.

Table 3 (continued)

MRL Materials ¹	Date Deposited	Date Tested	Atomic Solute %	Scan mV/sec	Eb (mV)	Ecorr (mV)	ip ($\mu\text{A}/\text{cm}^2$)	Comments
Al240.W(9-16).PC.Ar Al240.W(9-16).Si.Ar.1	2/2/94	2/9/94		0.2		-738		Scratches in center and edges seen prior to pol. After pol., all grey surface is seen (could be only Si left). No breakdown detected during pol.
Al240.W(9-16).PC.Ar Al240.W(9-16).Si.Ar.2	2/2/94	2/9/94		0.2		-730		After pol., a grey surface (probably Si) is left w/ 3 small dark circles. No breakdown detected during pol.
MMSS Materials	Date Deposited	Date Tested	Atomic Solute %	Scan mV/sec	Eb (mV)	Ecorr (mV)	ip ($\mu\text{A}/\text{cm}^2$)	Comments
pure Al		2/28/92	-----	0.2	-719	-1,081	~0.228	
Al480.Mo40.Si.Ar.1	7/20/92	2/25/93	20	0.2	885	-581	0.841	
Al480.Mo40.Si.Ar.2	7/20/92	2/26/93	20	0.2	461	-595	0.793	
graded Al-Mo.1		2/21/93	26 to 18	0.2	-627	-681		
graded Al-Mo.2		2/23/93	26 to 18	0.2	-505	-594	~0.118	
graded Al-Mo.3		3/24/93	26 to 18	0.05	-386	-620	0.229	

Notes:

1. Poly-carbonate (PC) sheets are used only for stress measurements.

* Composition is based on the average of alloys sputtered under identical conditions.

Table 4 Spot EDS Results of Selected Points Located in Figures 44 & 45.

Selected EDS Spot	Mo/Al Ratio
1	0.14
2	0.17
3	2
4	0.25
5	1.61
6	2.03
7	3.44
8	0
9	0.14

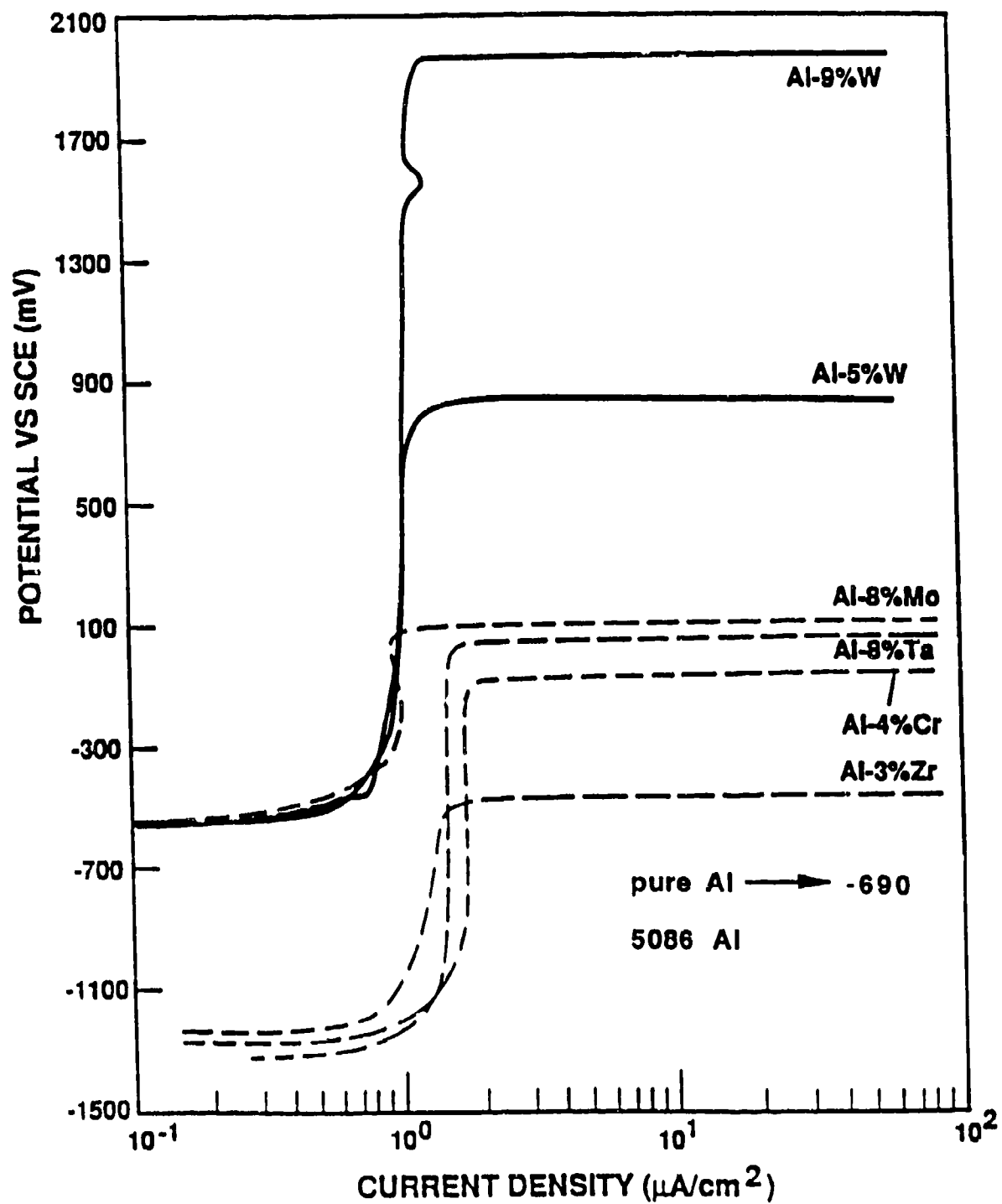


Figure 1. Anodic Polarization Behavior for Stainless AL Alloys in Aerated 0.1M KCl at 25 C.

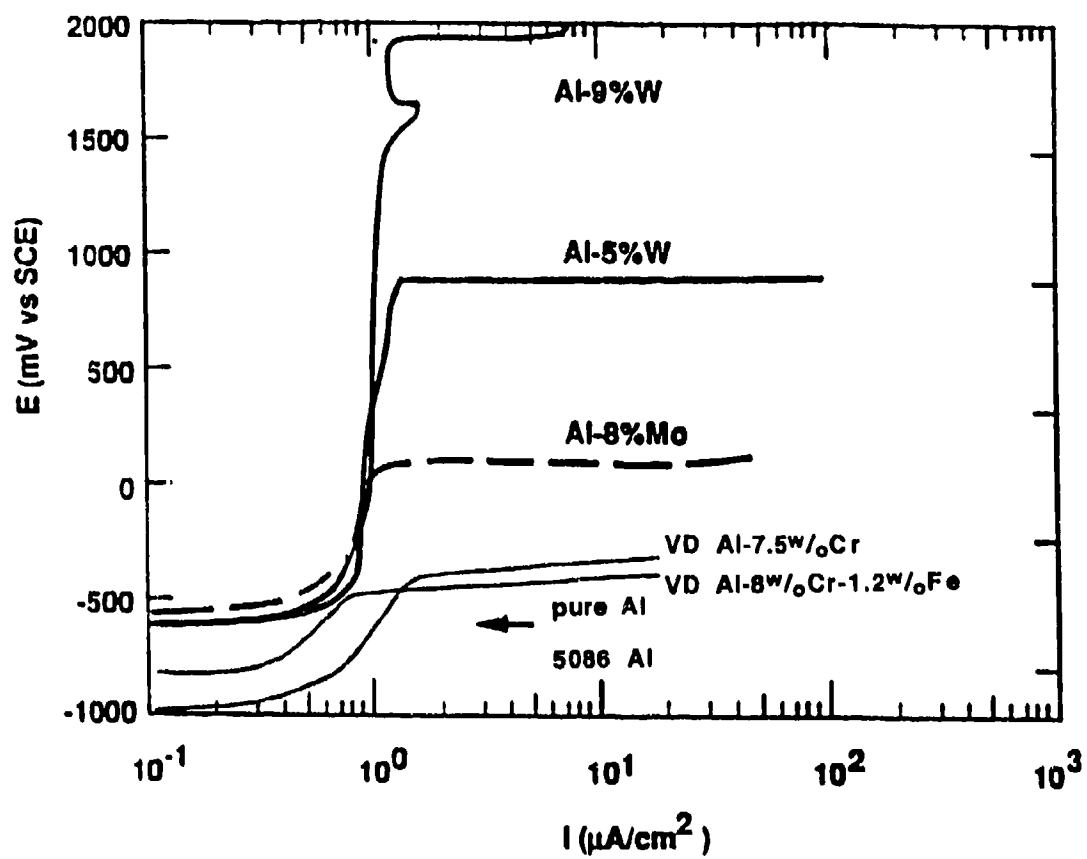


Figure 2. Comparison of Anodic Polarization Behavior for RAE and Stainless AL Alloys in Aerated 0.1M KCl at 25 C.

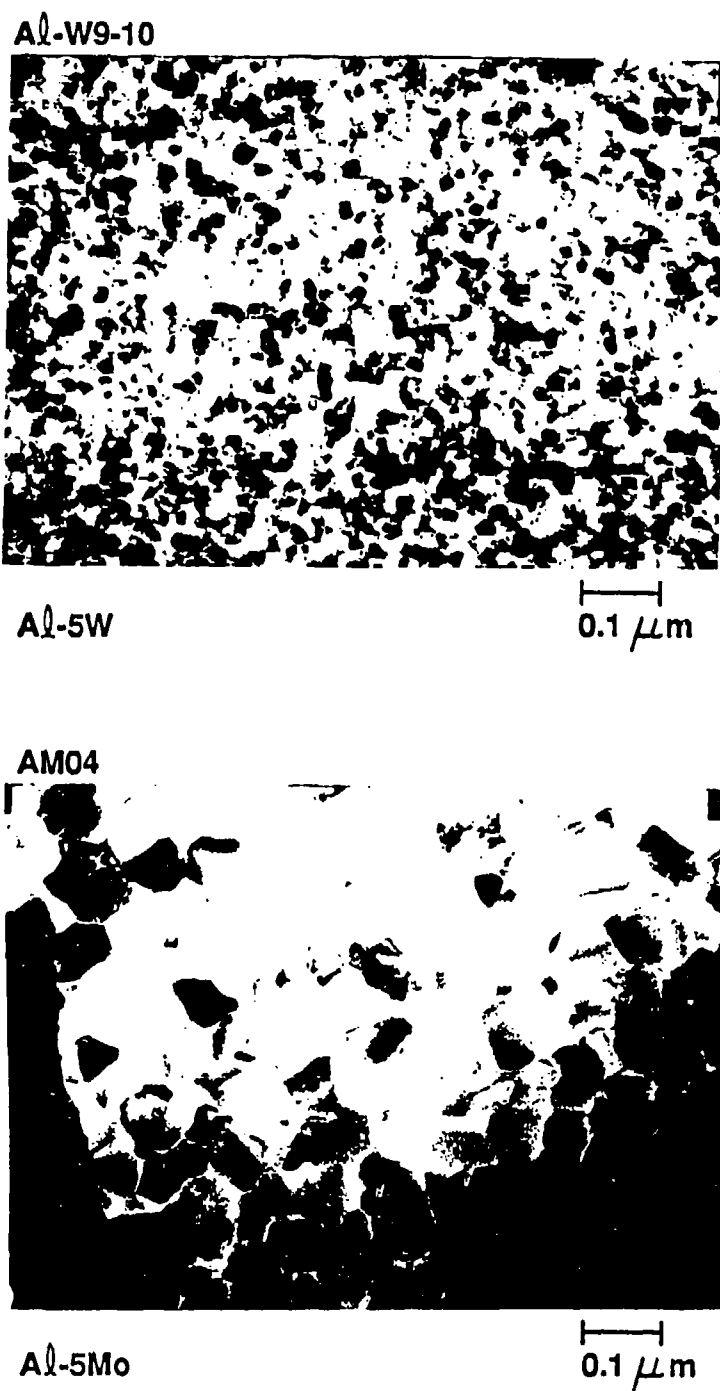


Figure 3. TEM Micrographs of an Al-5%Mo Specimen and an Al-5%W Specimen.

Al-W

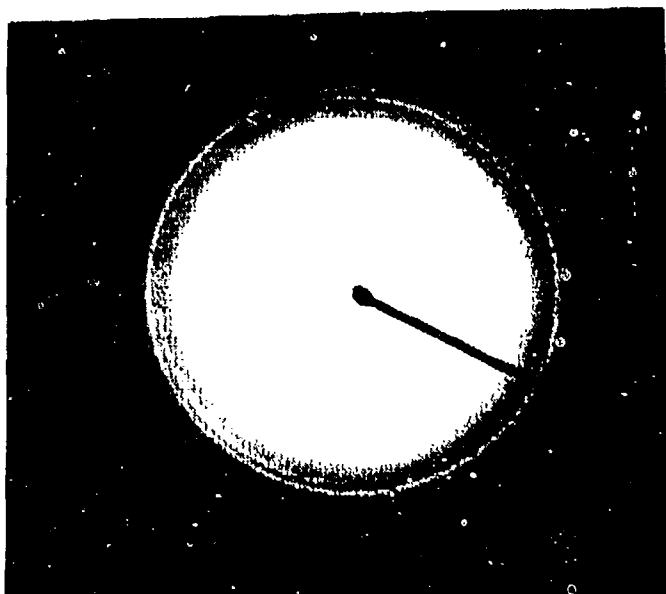
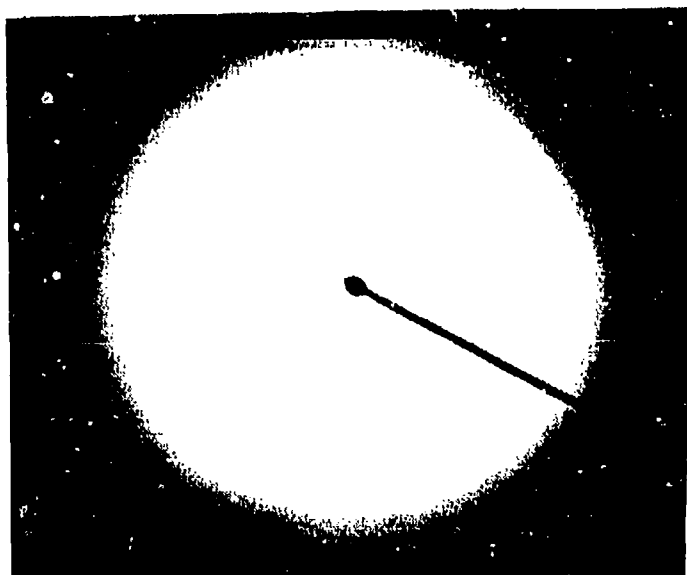
**Crystalline****Amorphous**

Figure 4. Selected Area Electron Diffraction Patterns for a Crystalline Al-W Specimen and an Amorphous Al-W Specimen ($[W] > 9\%$).

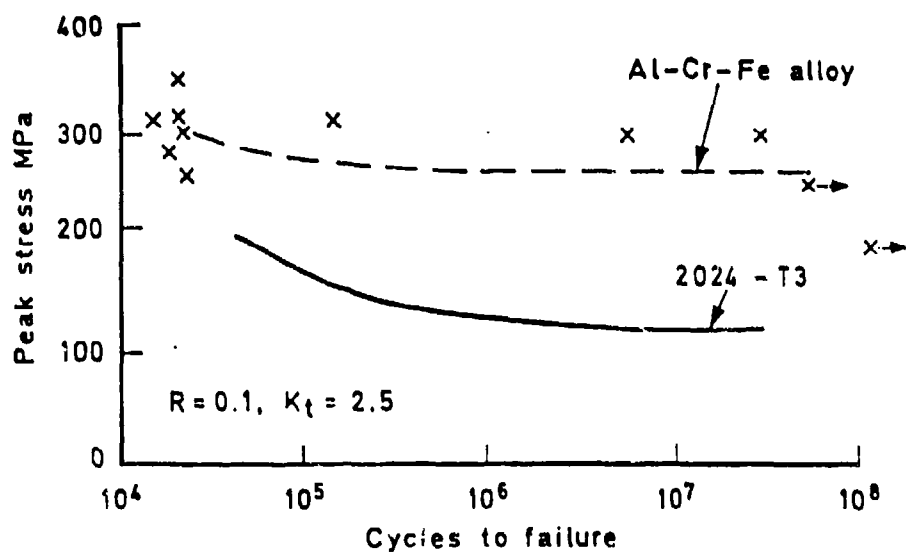


Figure 5. Constant Amplitude Fatigue Data, L-T Orientation, for Sheet Type Test Pieces¹².

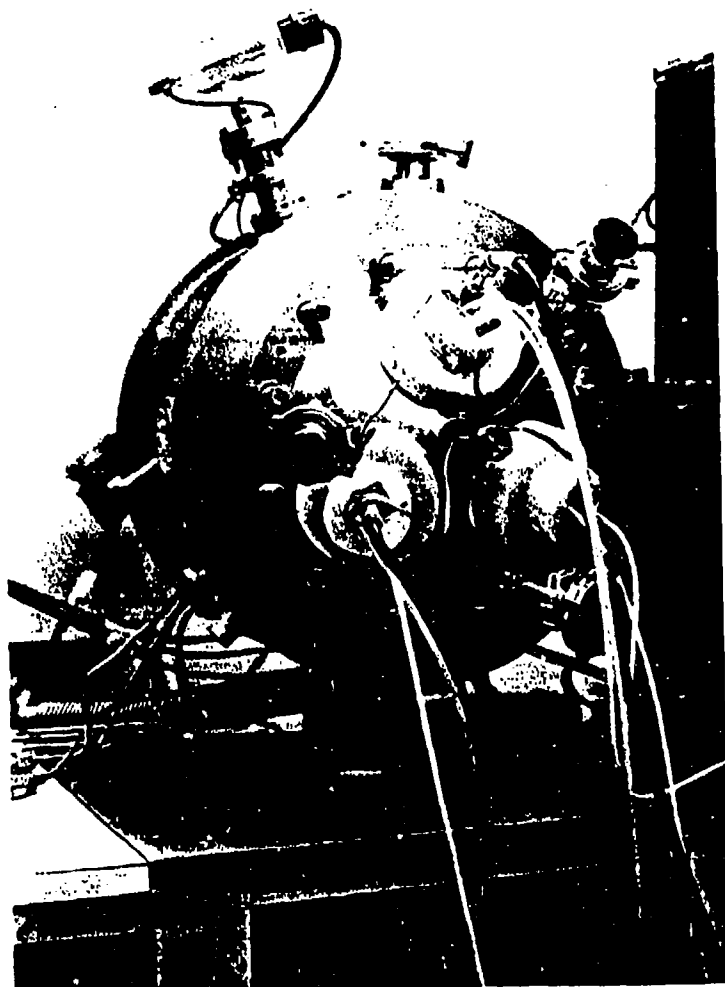


Figure 6. PSU Sputter Deposition System.

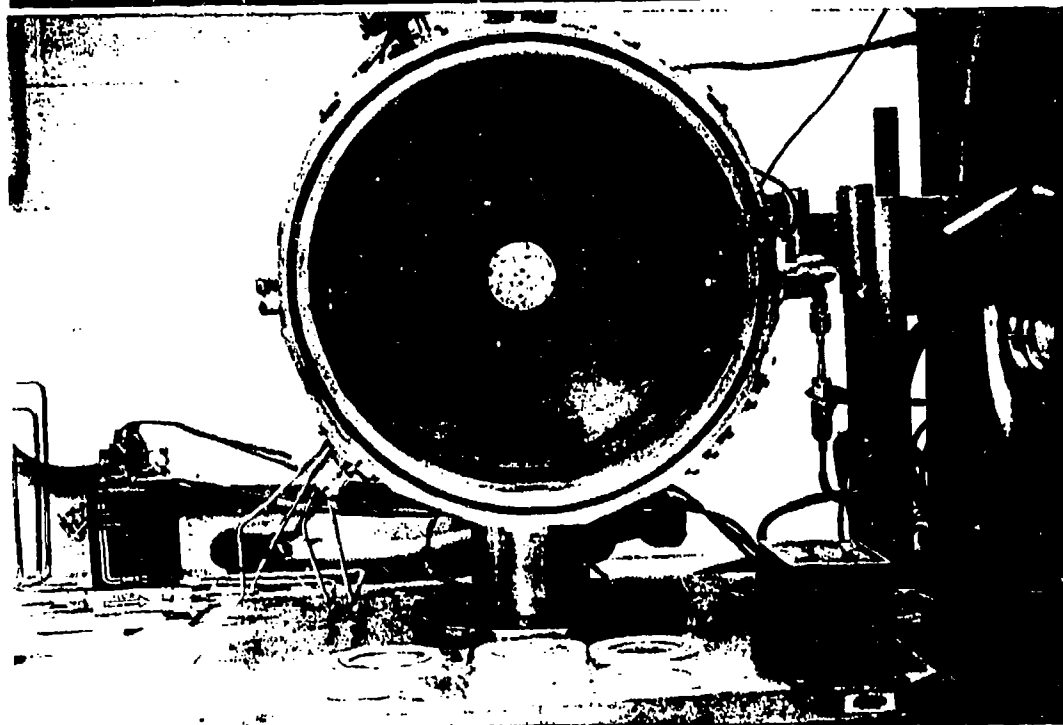


Figure 7. Position of Sample Mount and Targets inside Chamber.

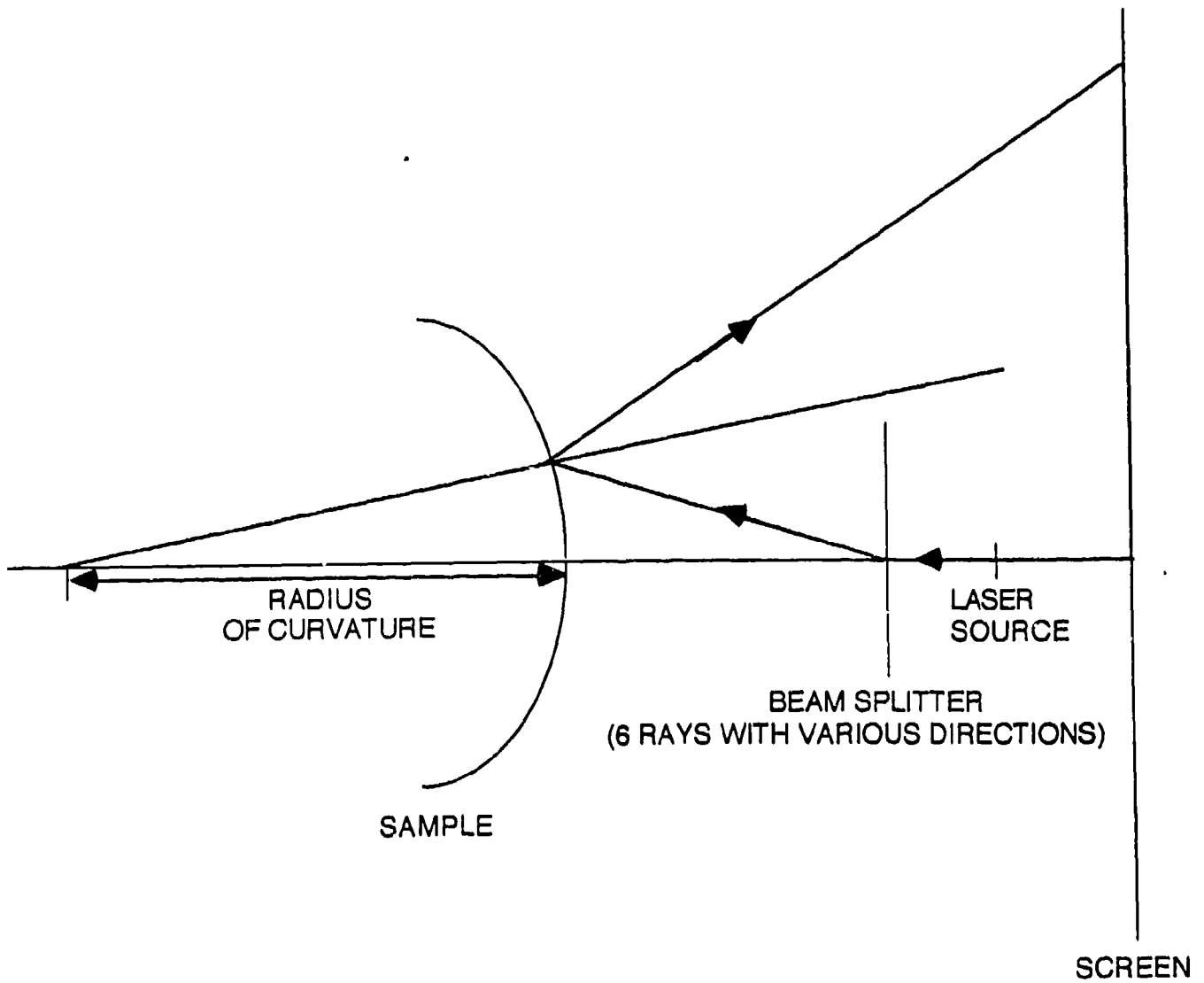


Figure 8. Residual Stress Measurement Method.

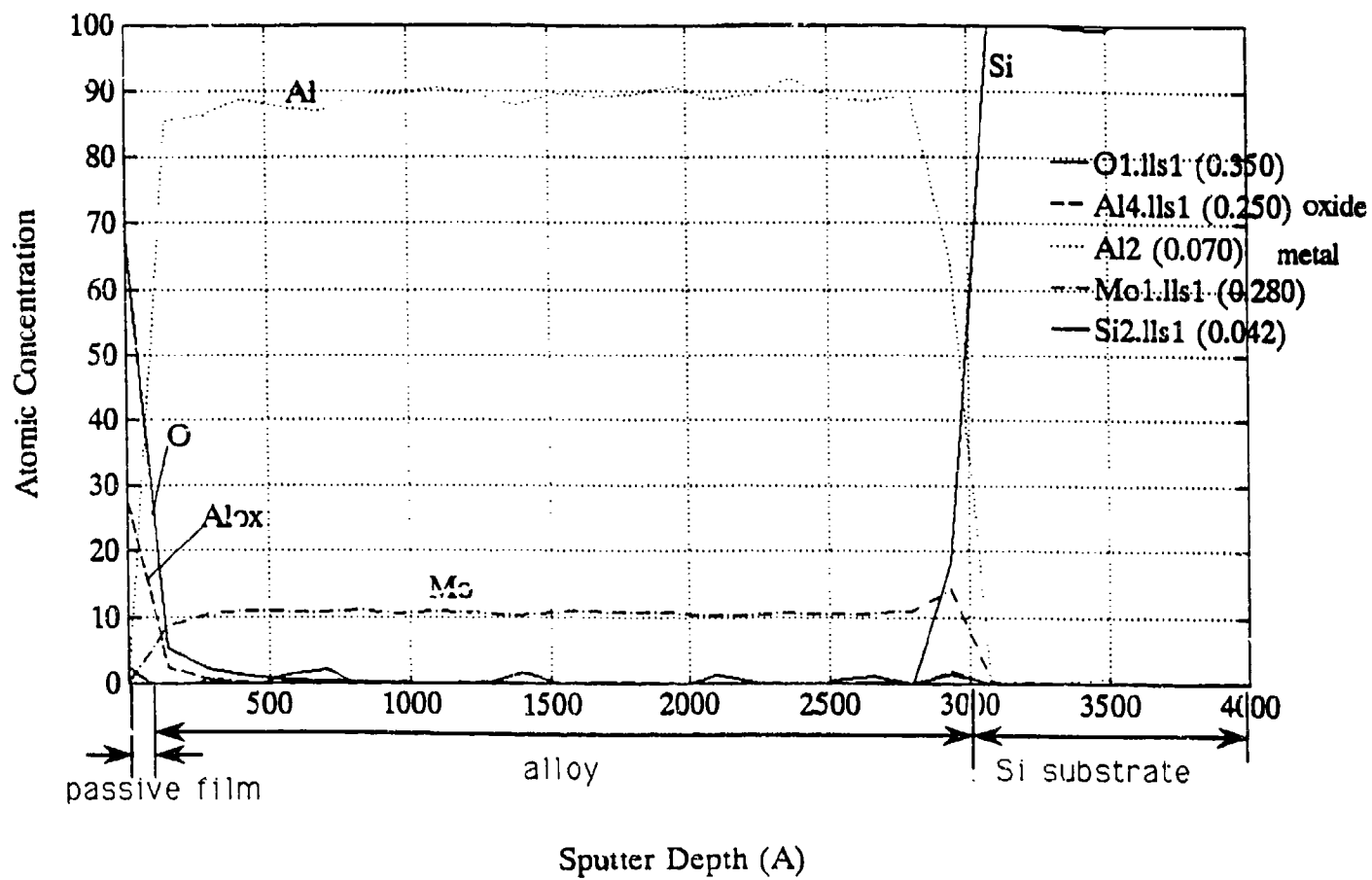


Figure 9. Auger Result of as-deposited Al - 9%Mo.

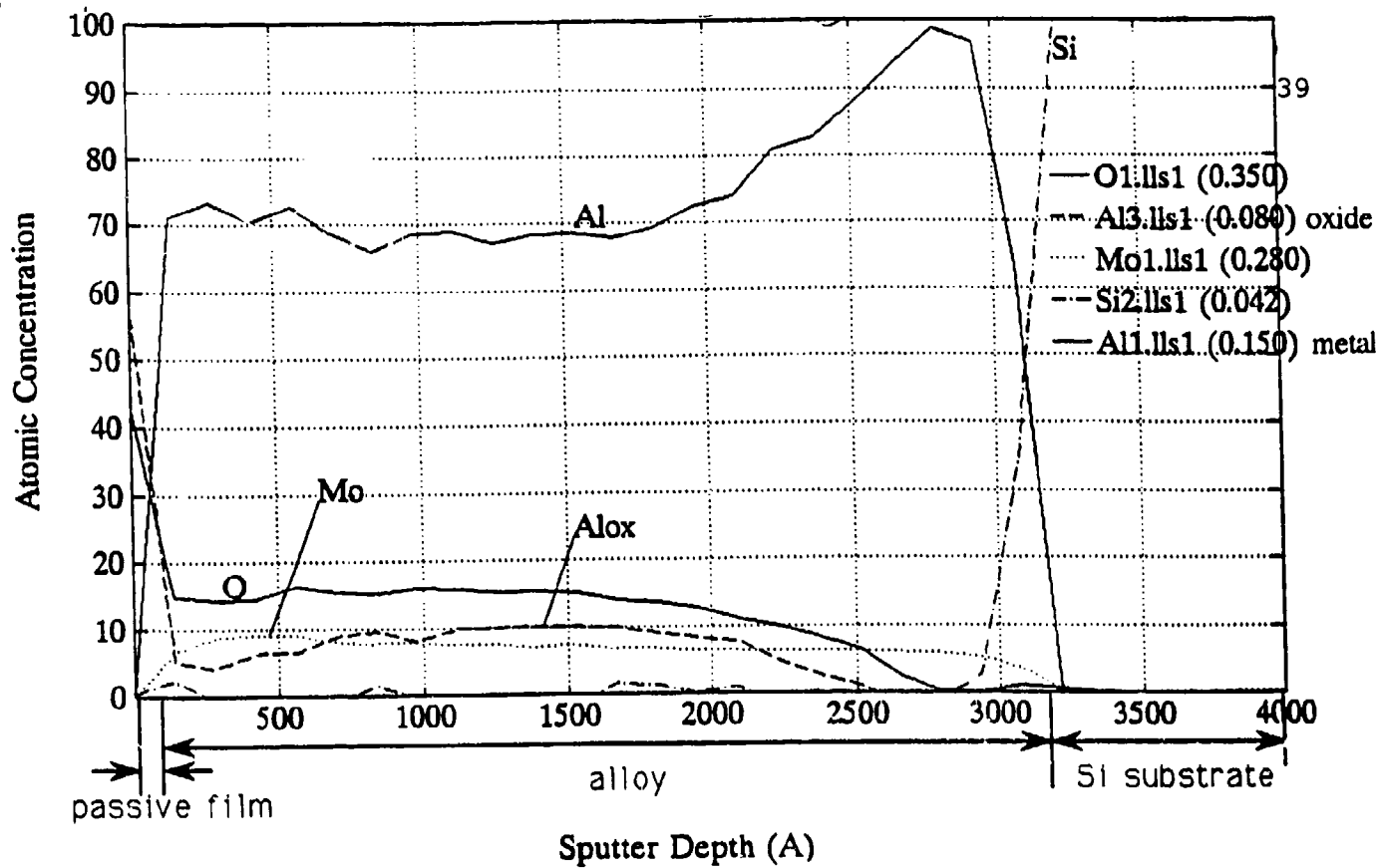


Figure 10. Auger Result of as-deposited Al - (3% to 9%) Mo.

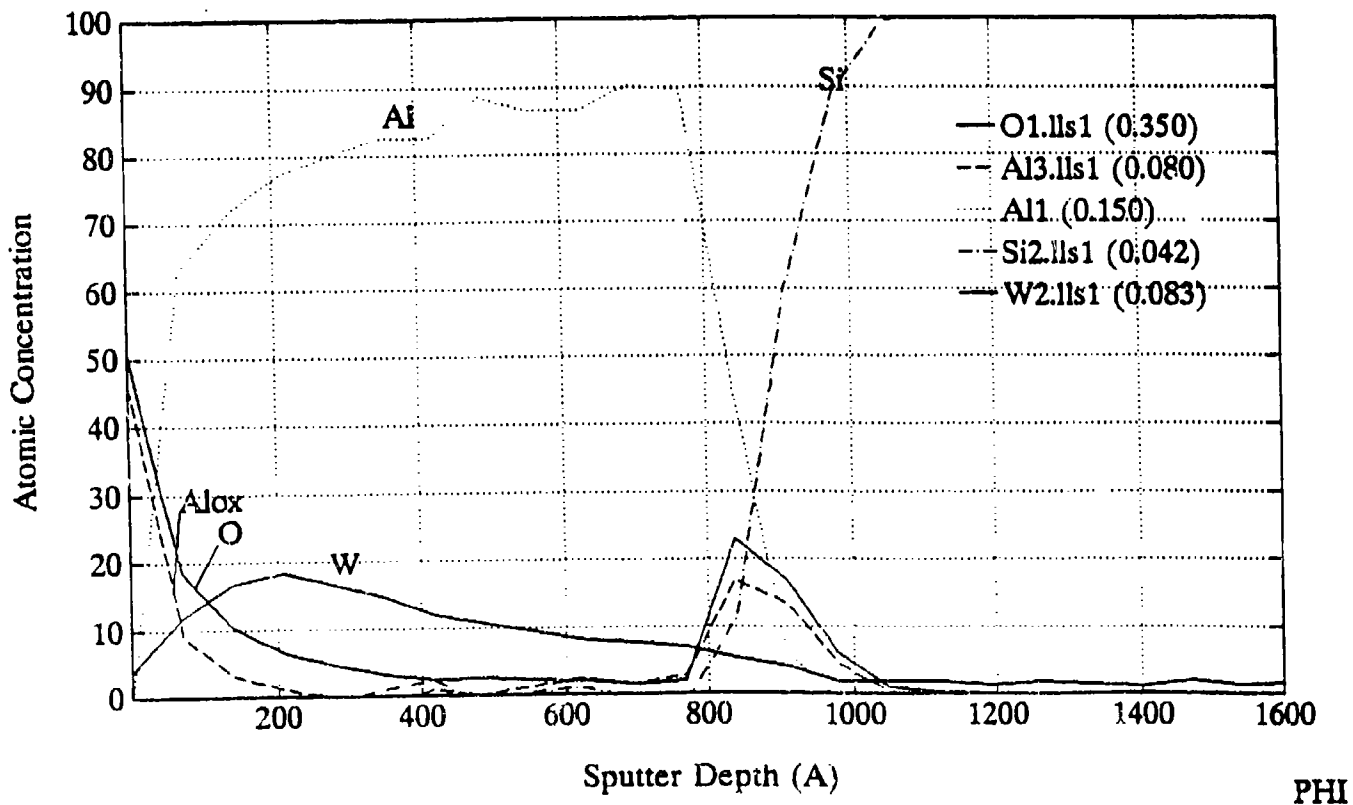


Figure 11. Auger Result of as-deposited Al - (0% to 14%) W.

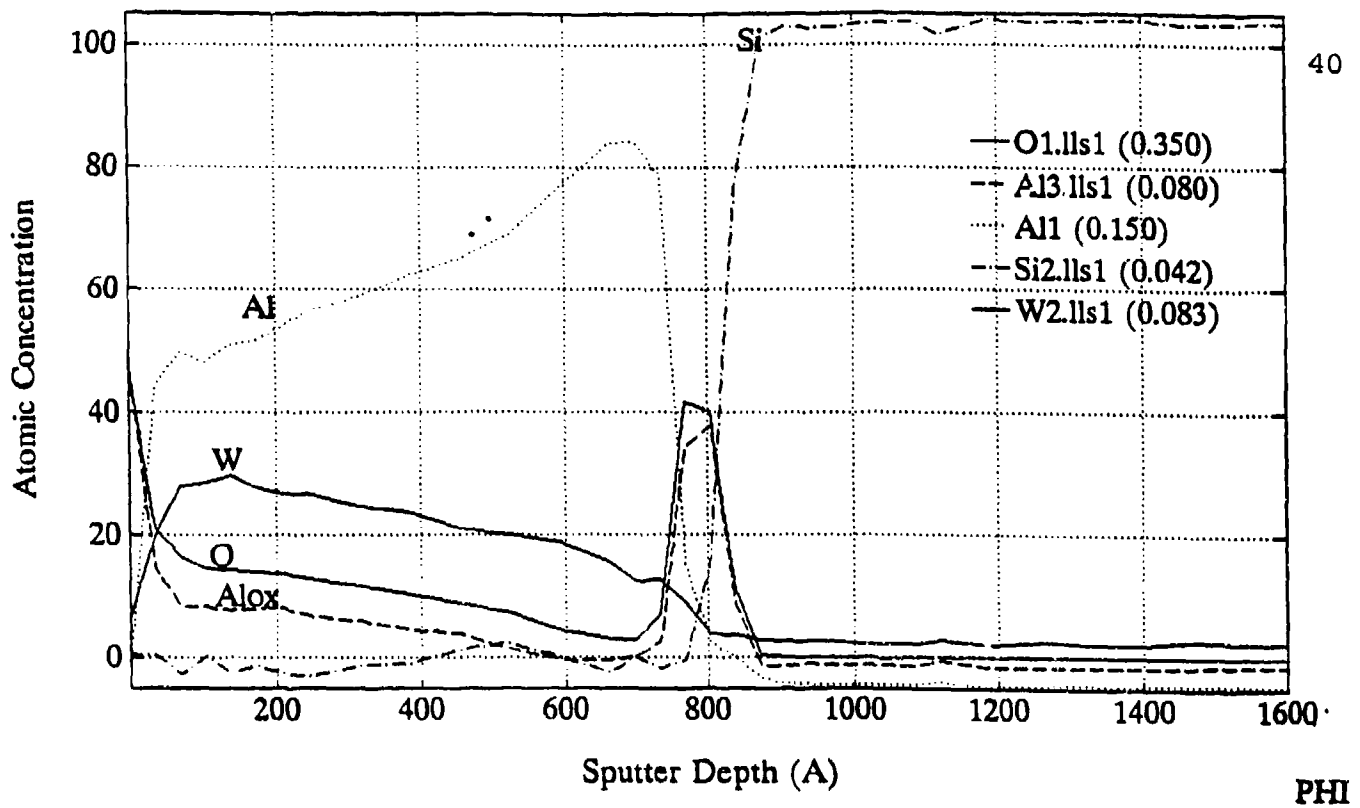


Figure 12. Auger Result of as-deposited Al - (0% to 13%)W.

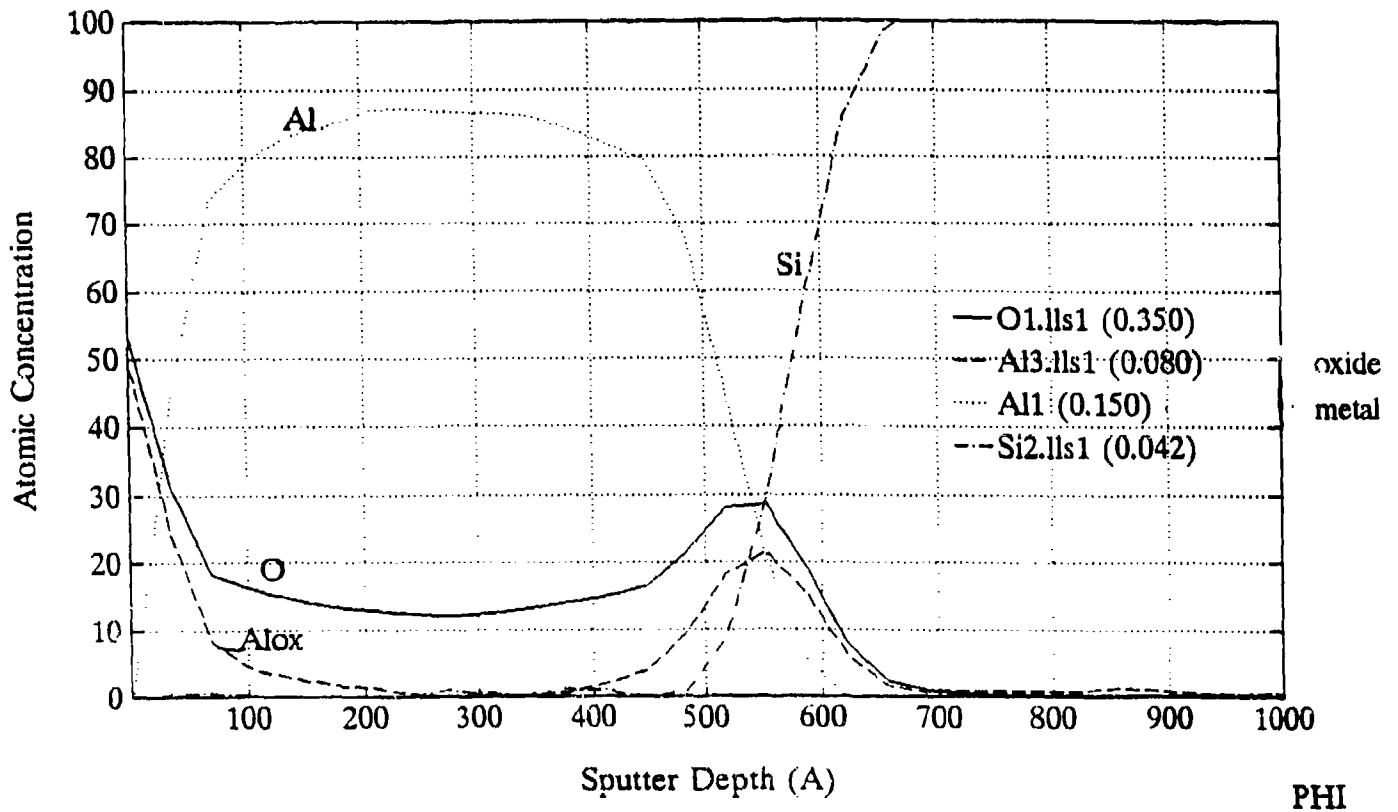


Figure 13. Auger Result of as-deposited pure Al (120 Watt). Further analysis of the raw data shows slight presence of Al_2O_3 throughout film. The detected O comes from the Al_2O_3 .

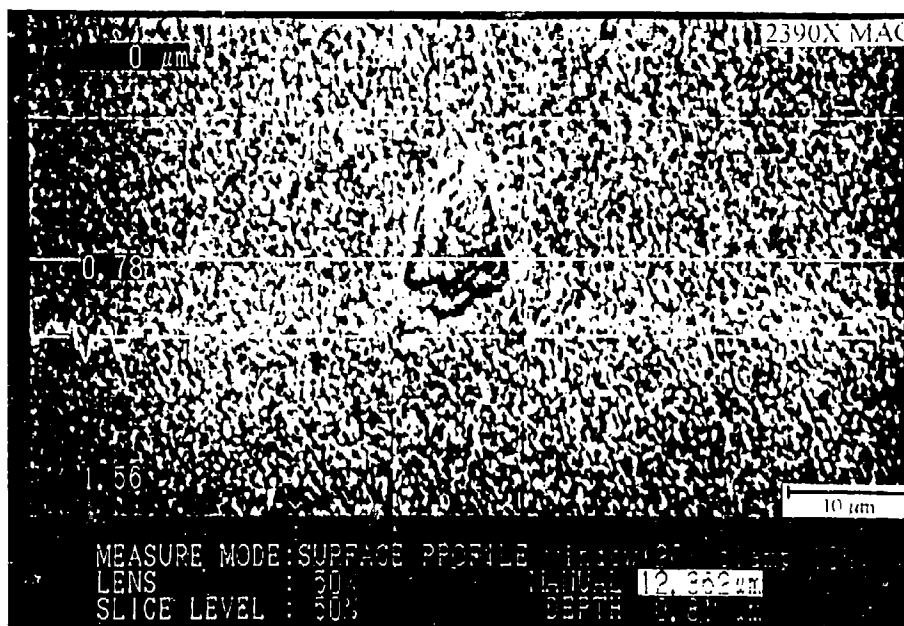


Figure 16. SLM Photo of Defect on an as-deposited Al - 3% Mo Alloy.

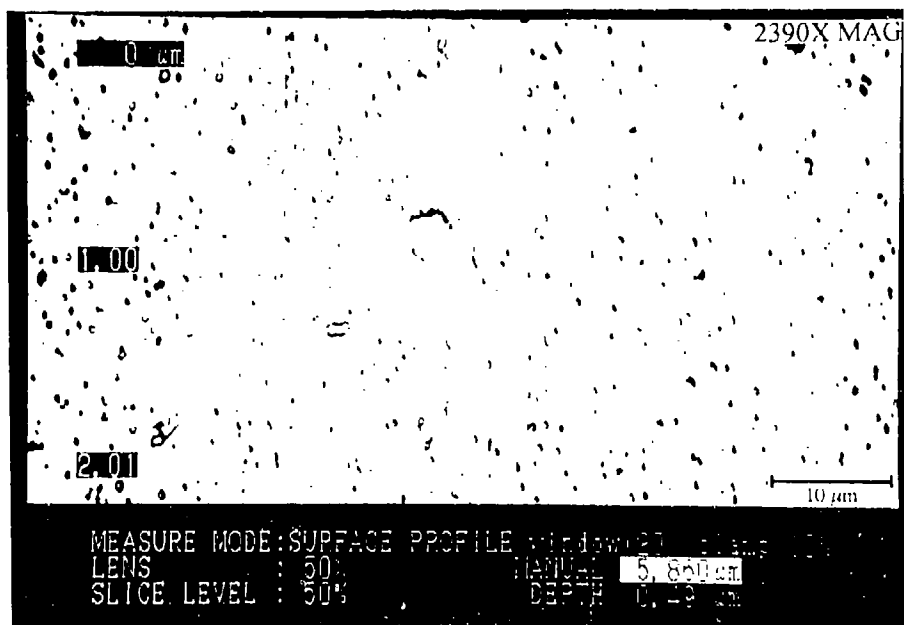


Figure 17. SLM Photo of Defect on an as-deposited Sputter Deposited Pure Al.

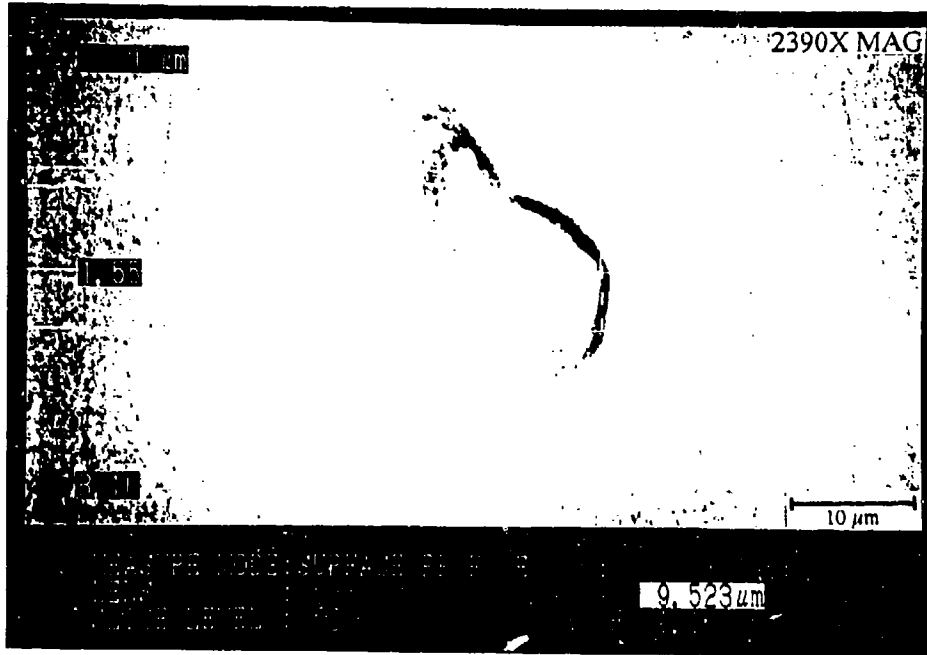


Figure 18. SLM Photo of a Defect on an as-deposited Al - 6.5% Ta Alloy.

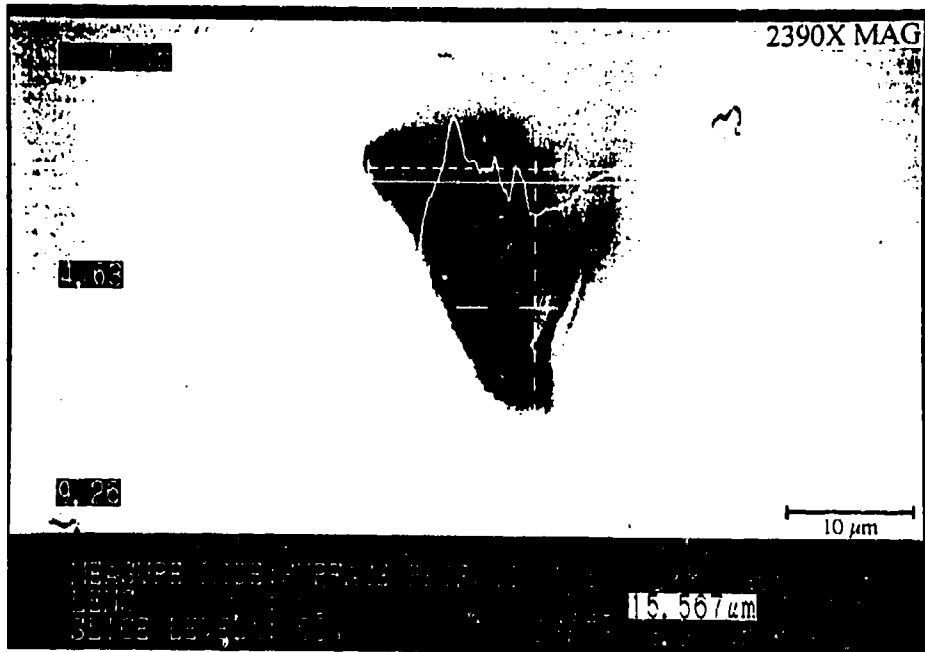


Figure 19. SLM Photo of a Defect on an as-deposited Al - (approx. 10%) W. Alloy.

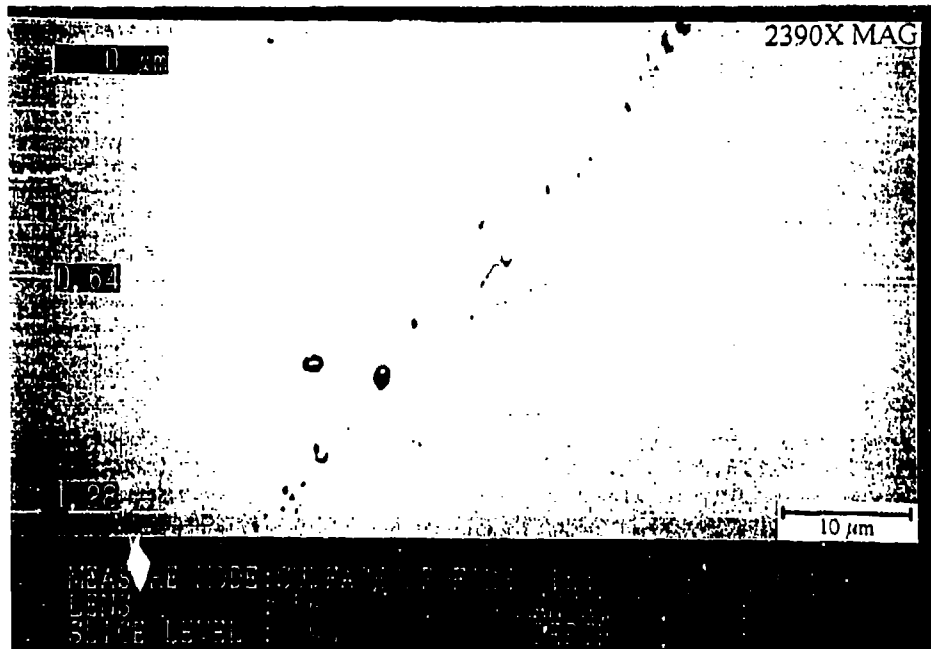


Figure 20. SLM Photo of a Defect on as-deposited Al - (0 to 14%) W Alloy.

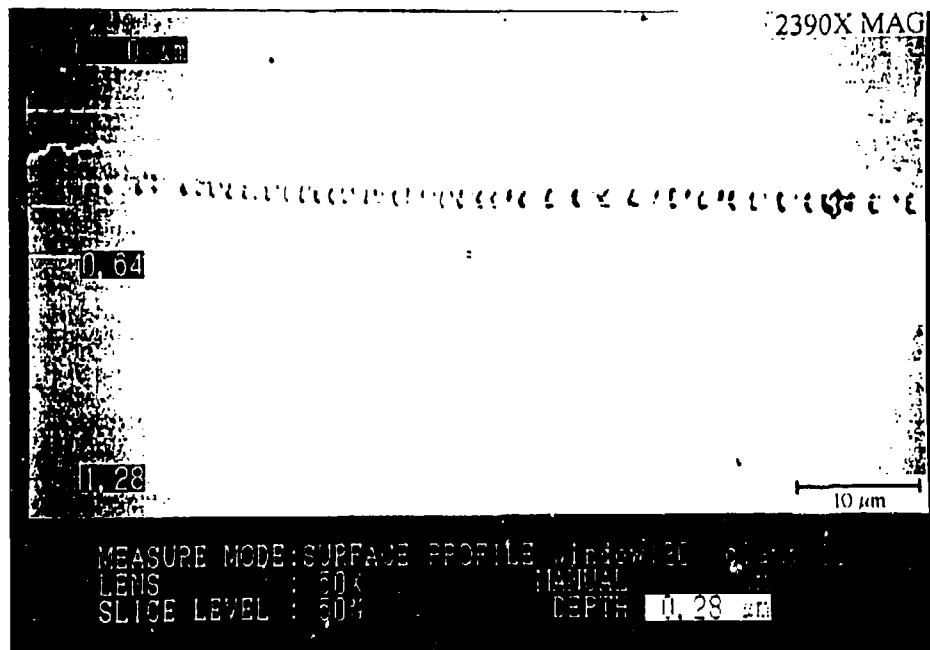


Figure 21. SLM Photo of a Defect on an as-deposited Al - (0 to 14%) W Alloy.

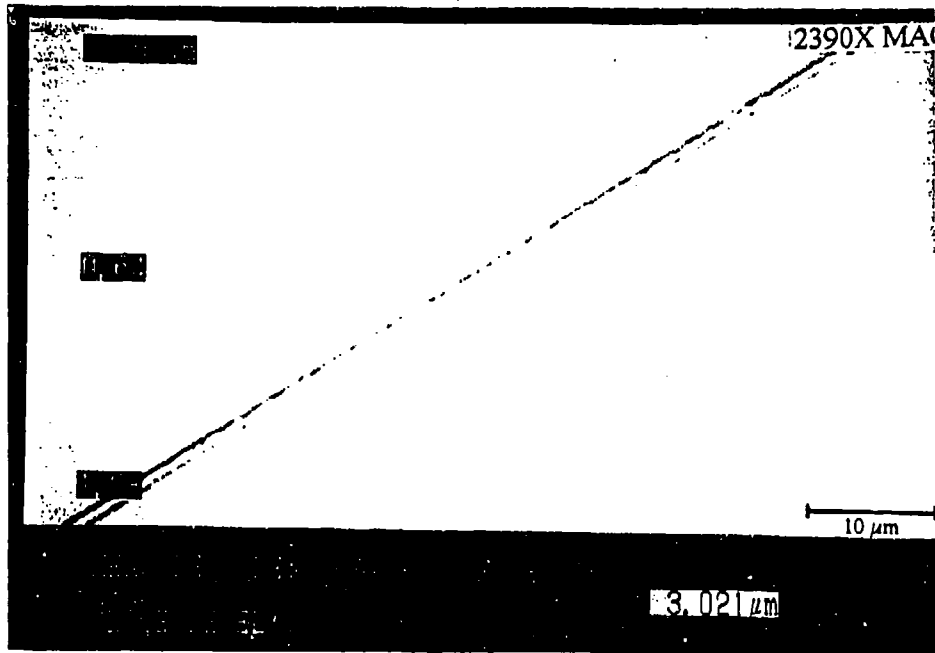


Figure 22. SLM Photo of a Scratch on an Unclean, Cleaved Silicon Substrate.

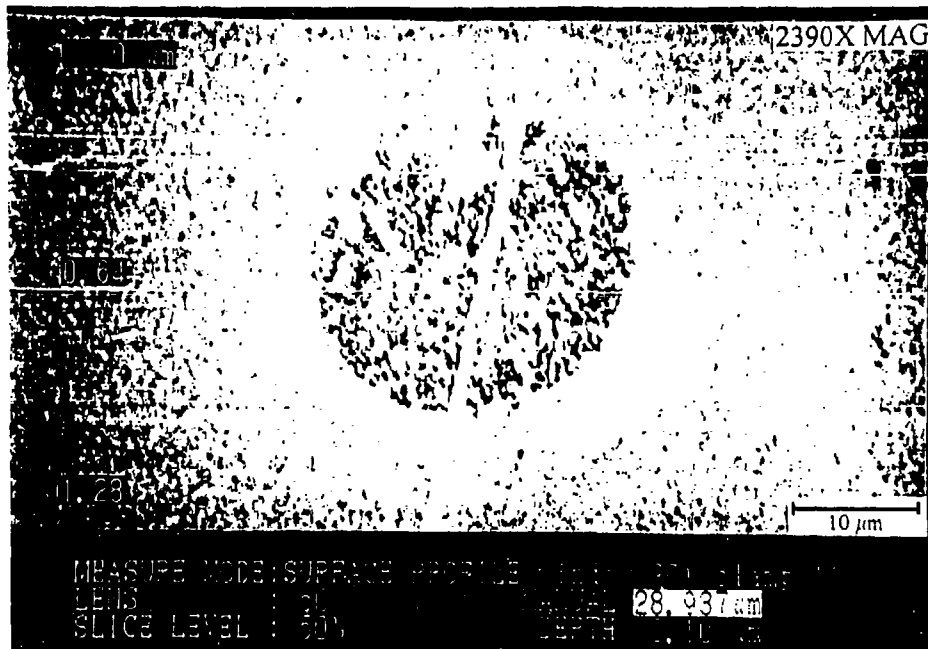


Figure 23. SLM Photo of Defect on an as-deposited Al - 6.5% Ta Alloy.

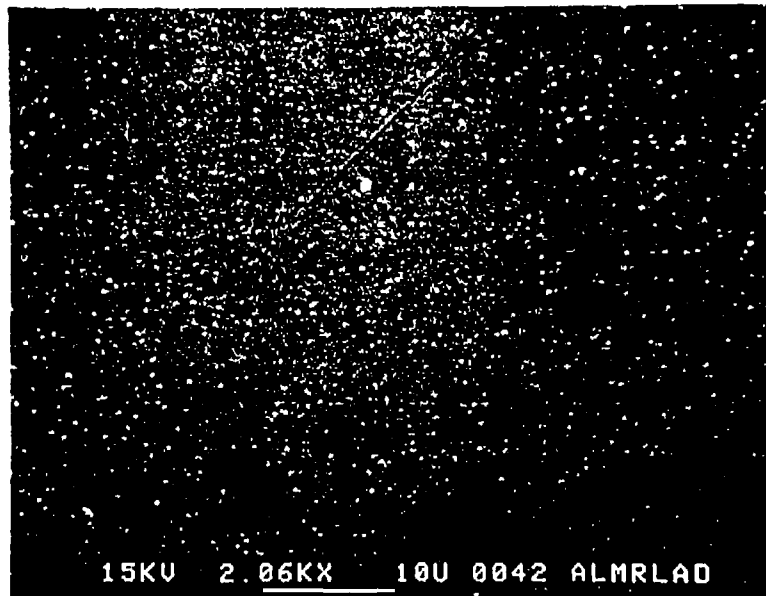


Figure 24. HSEM Micrograph of an as-deposited MRL Pure Al Film.

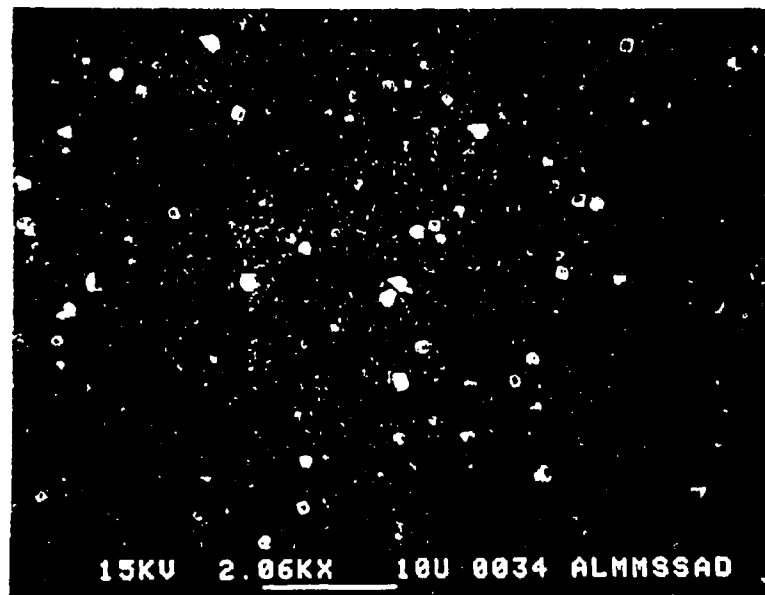


Figure 25. HSEM Micrograph of an as-deposited MMSS Pure Al Film.

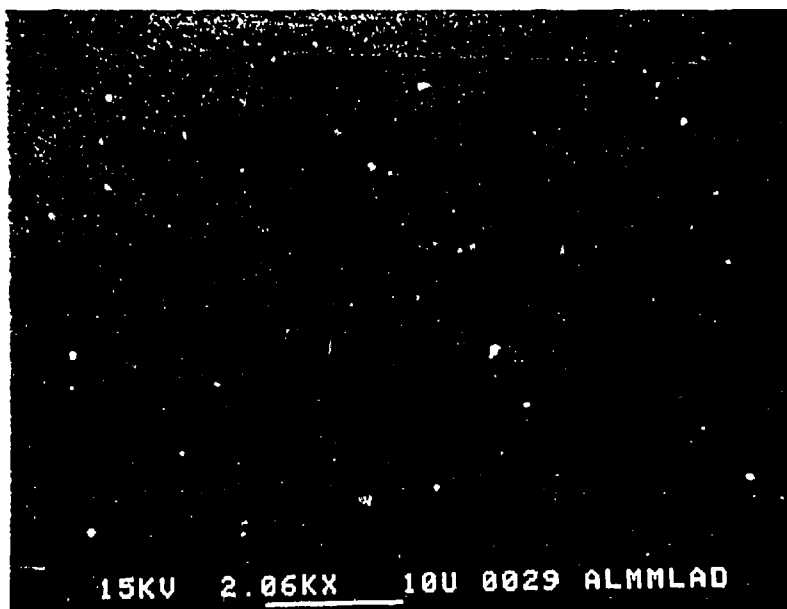


Figure 26. HSEM Micrograph of an as-deposited MML Pure Al Film.

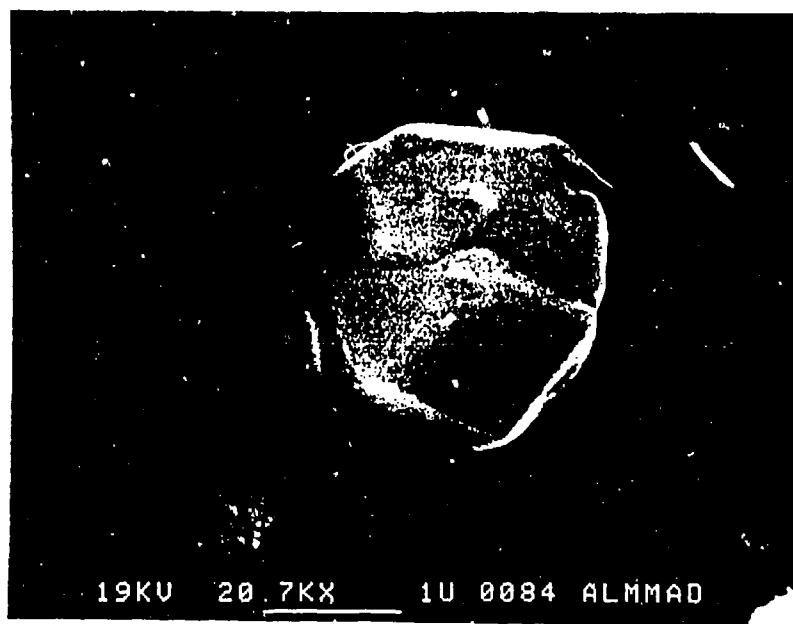


Figure 27. HSEM Micrograph of an Enlargement of a Large White Grain, seen in Figure 25.

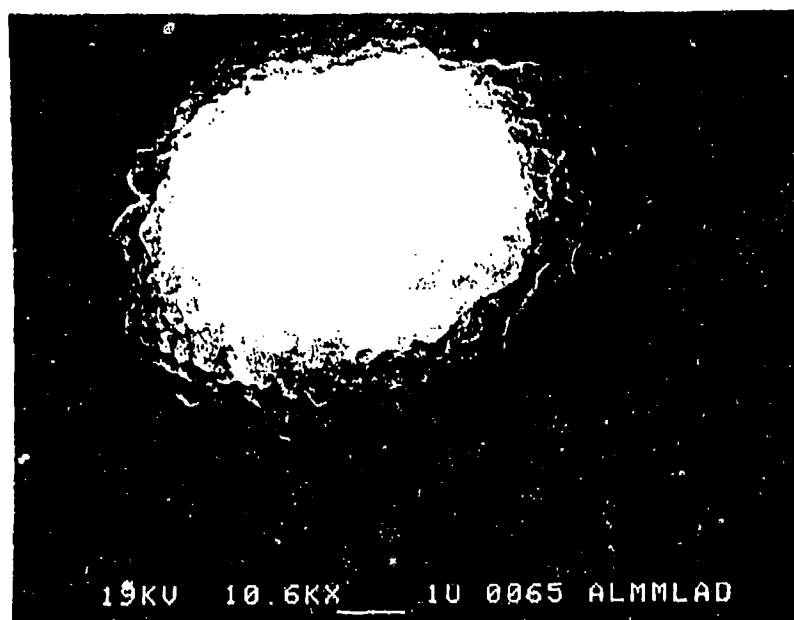


Figure 28. HSEM Micrograph of Enlargement of a Large White Growth, seen in Figure 26.

Al-W (120 Watt Al)

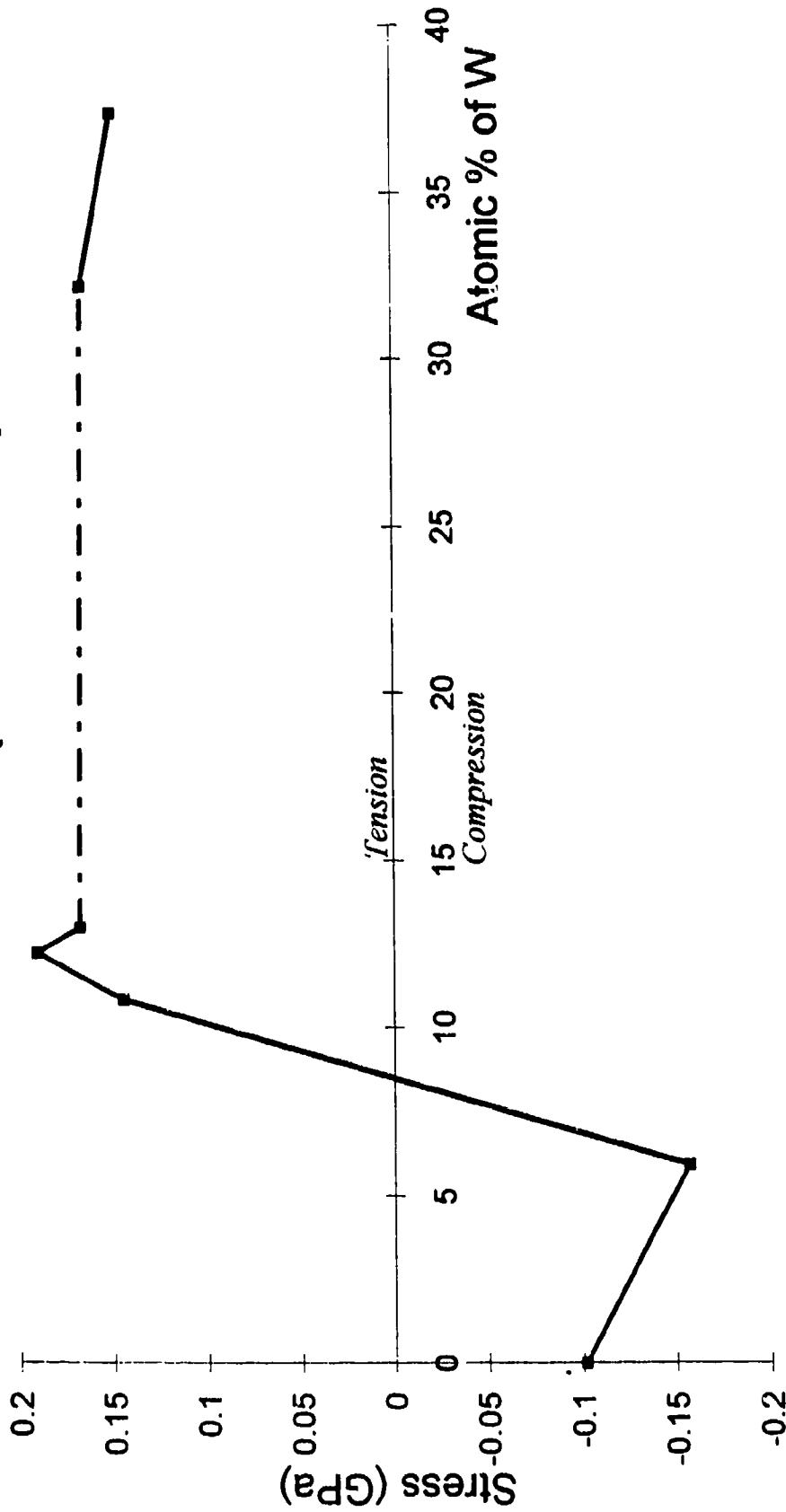


Figure 29. Residual Stress vs. Solute Concentration for Al-W
(Power Setting for Al target was 120W).

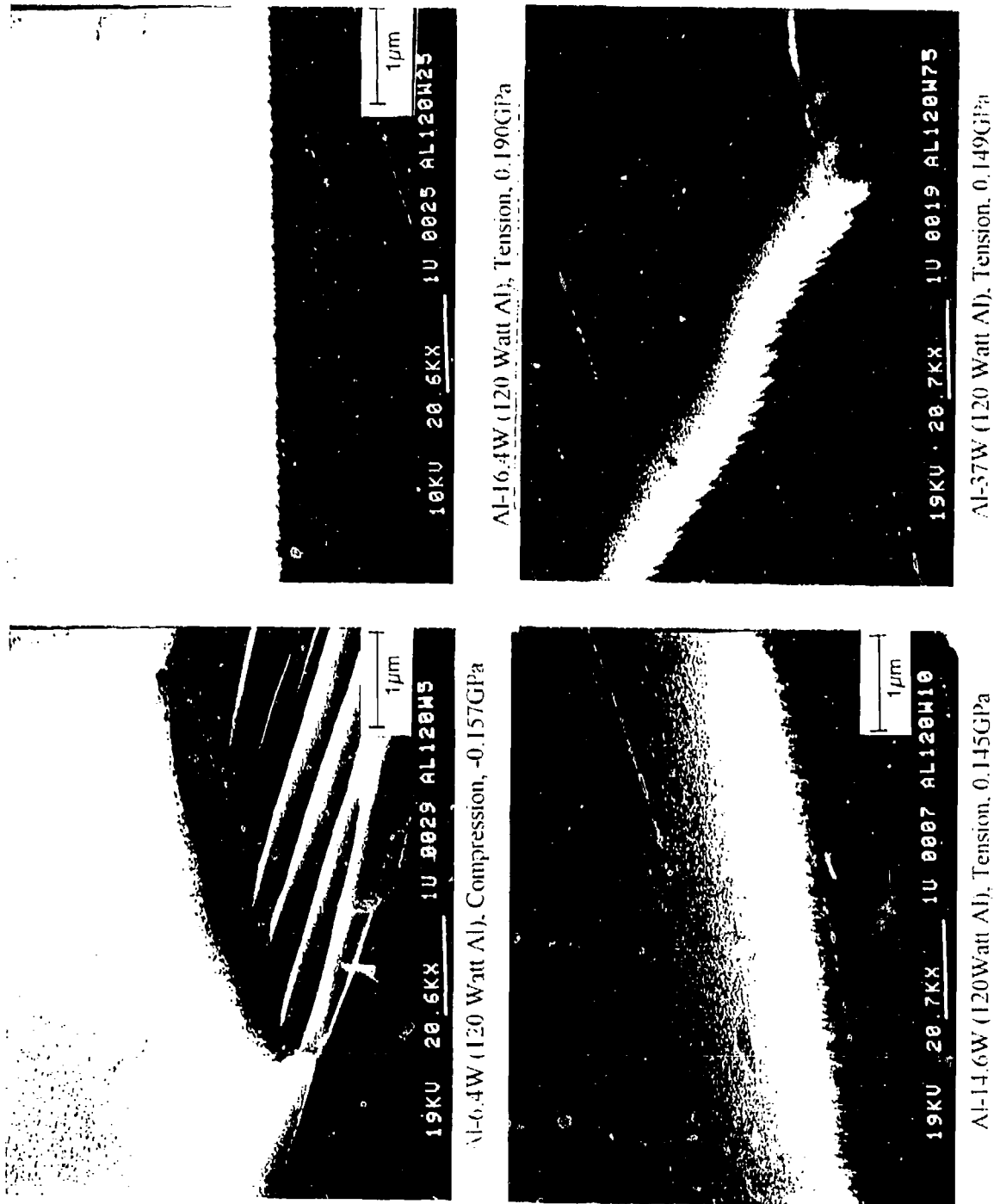


Figure 30. Cross-Sectional Microstructure for Al 120 Watt-W Alloys:
 (a) 6.4% W, (b) 14.6% W, (c) 16.4% W, (d) 37% W.

Al-W (240 Watt Al)

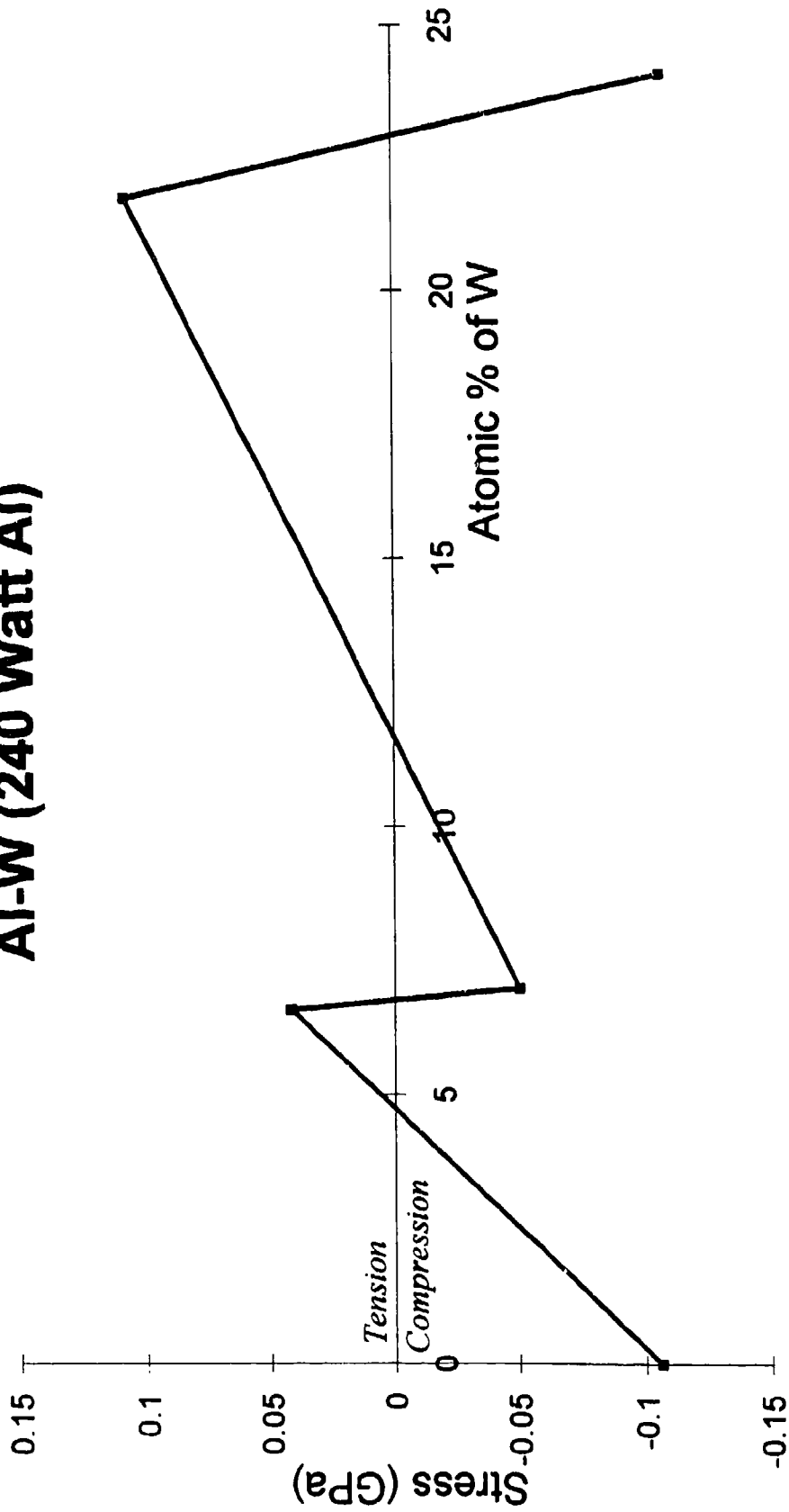
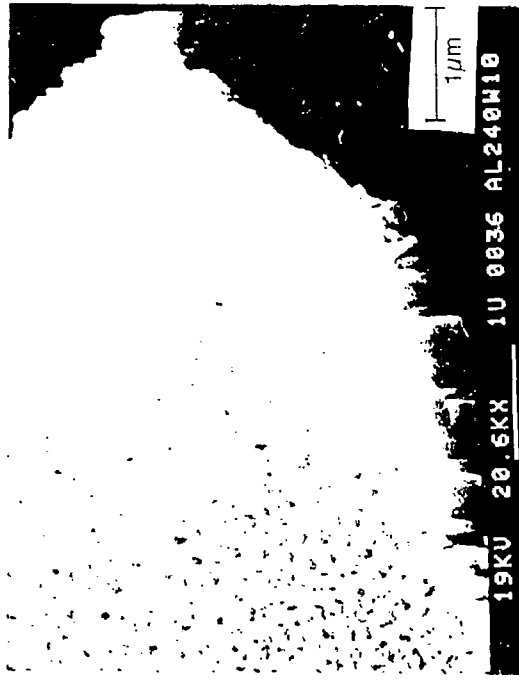
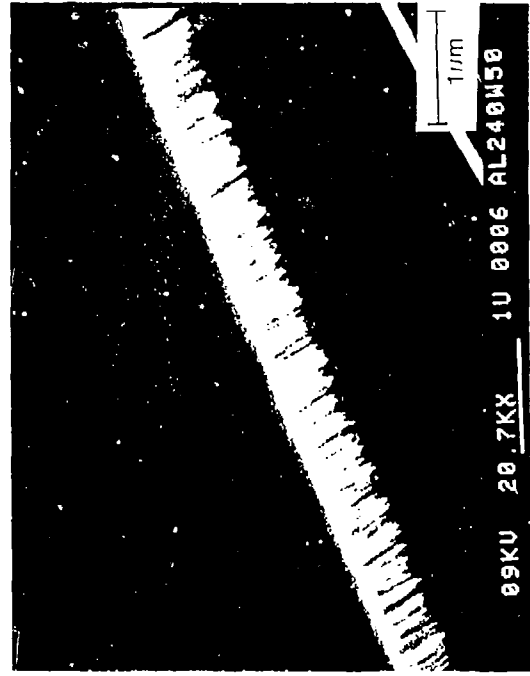


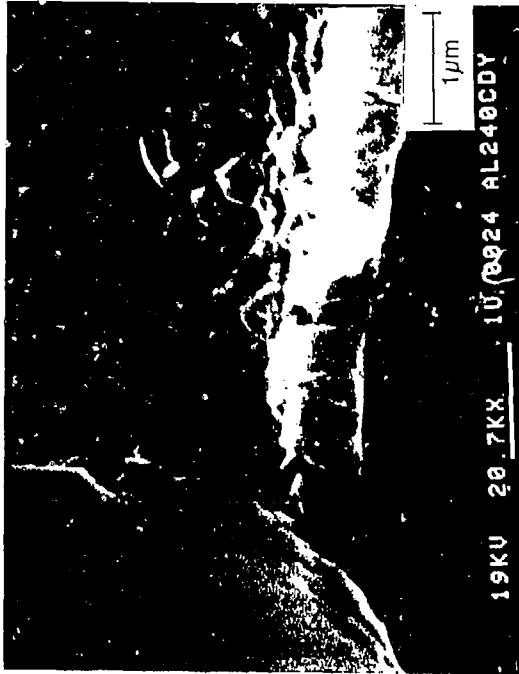
Figure 31. Residual Stress vs. Solute Concentration for Al-W (Power Setting for the Al target was 240 W).



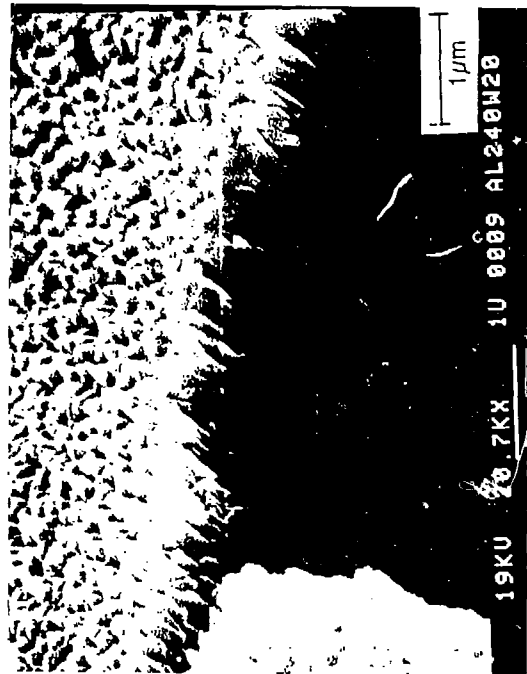
Al-7W (240 Watt Al), Compression, -0.050GPa



Al-22W (240 Watt Al), Tension, 0.107GPa



pure Al (240 Watt Al), Compression, -0.106GPa



Al-6.6W (240 Watt Al), Tension, 0.042GPa

Figure 32. Cross-Sectional Microstructure of Al 240 Watt-W Alloys:
(a) 0% W, (b) 6.6% W, (c) 7% W, (d) 22% W.

Al-Mo (240 Watt Al)

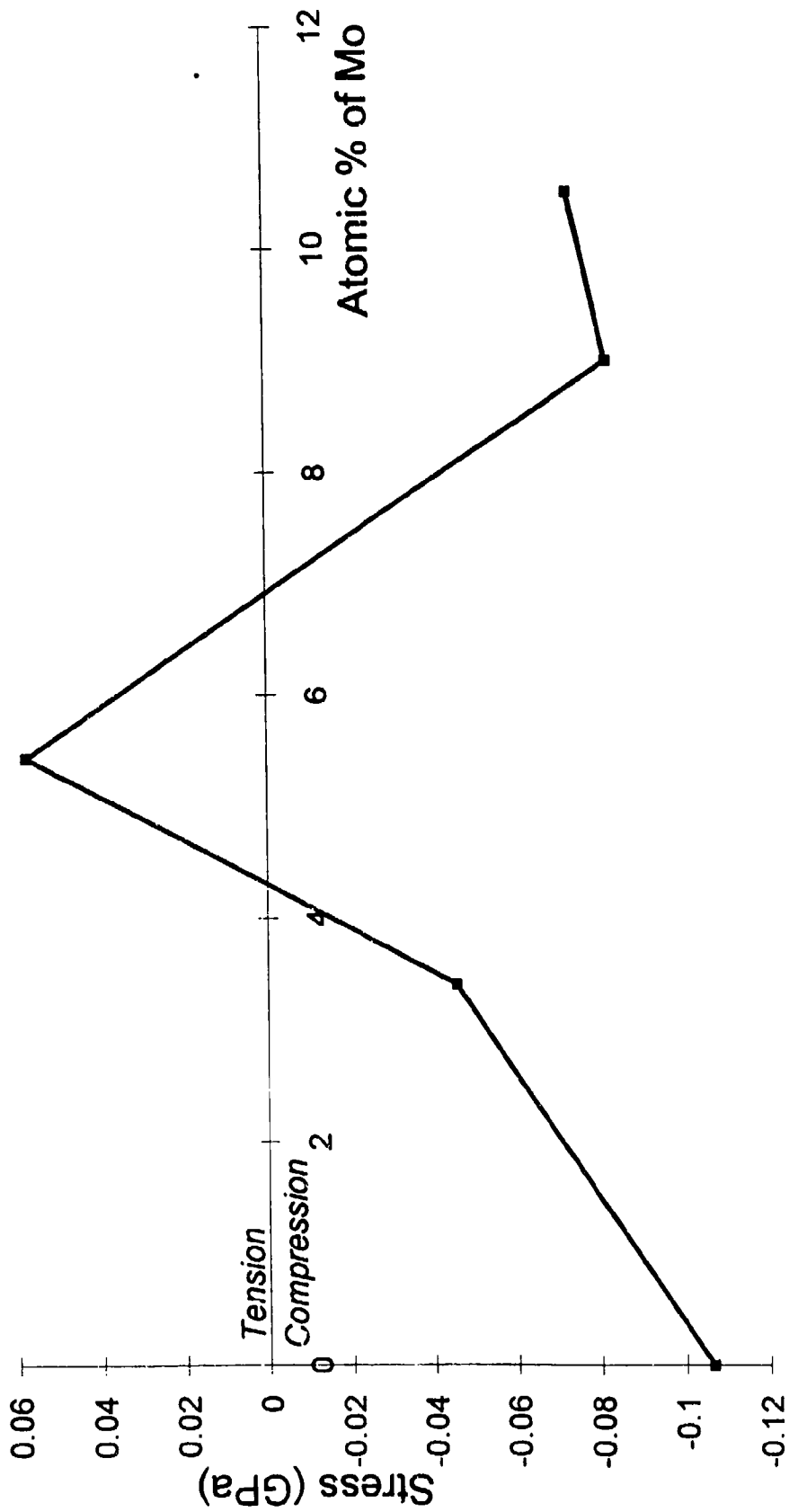


Figure 33. Residual Stress vs. Solute Concentration for Al-Mo (Power Setting for the Al target was 240 W).

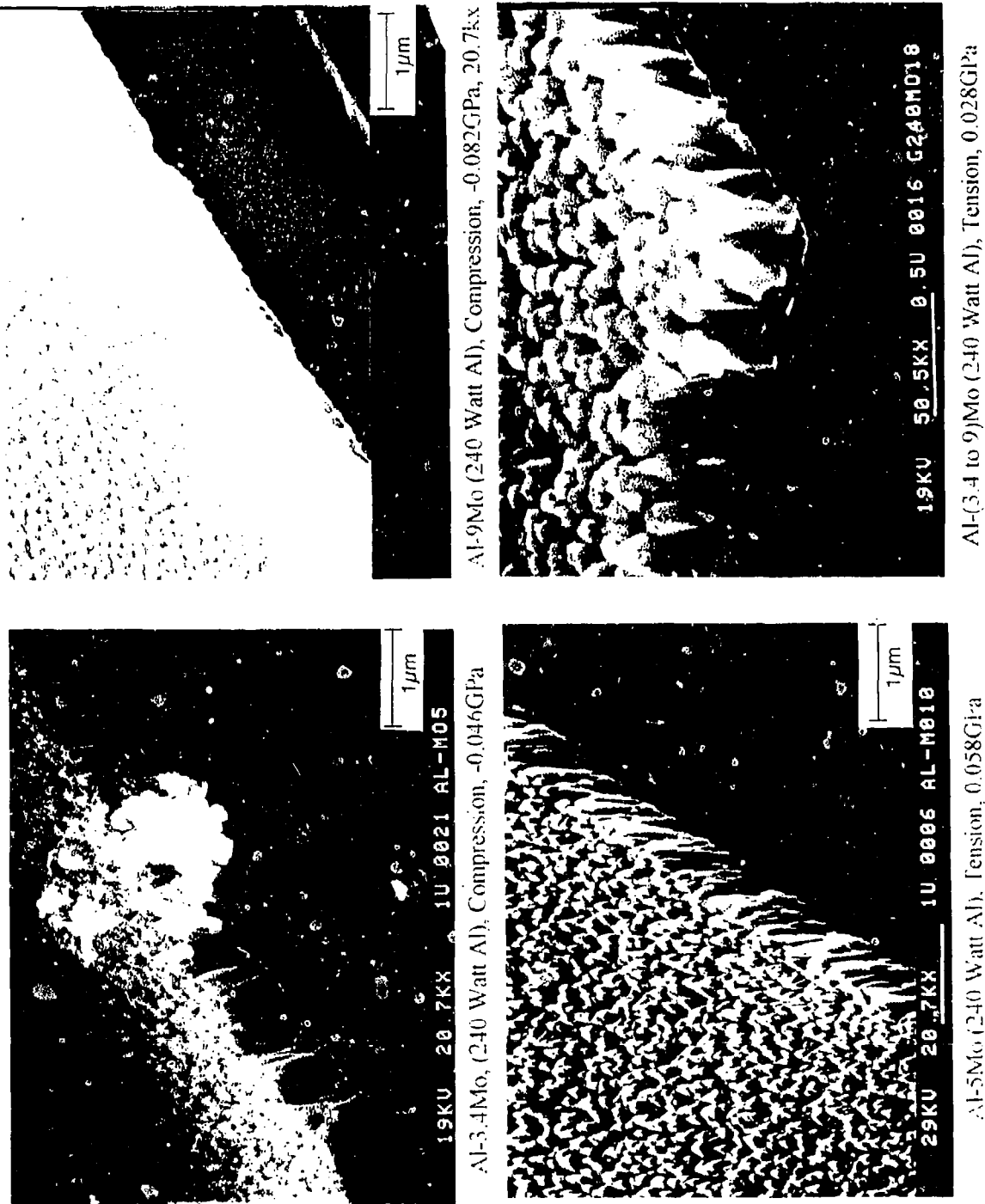


Figure 34. Cross-Sectional Microstructure of Al-240 Watt Mo Alloys.
 (a) 3.4% Mo, (b) 5% Mo, (c) 9% Mo, (d) (3.4 to 9)% Mo.

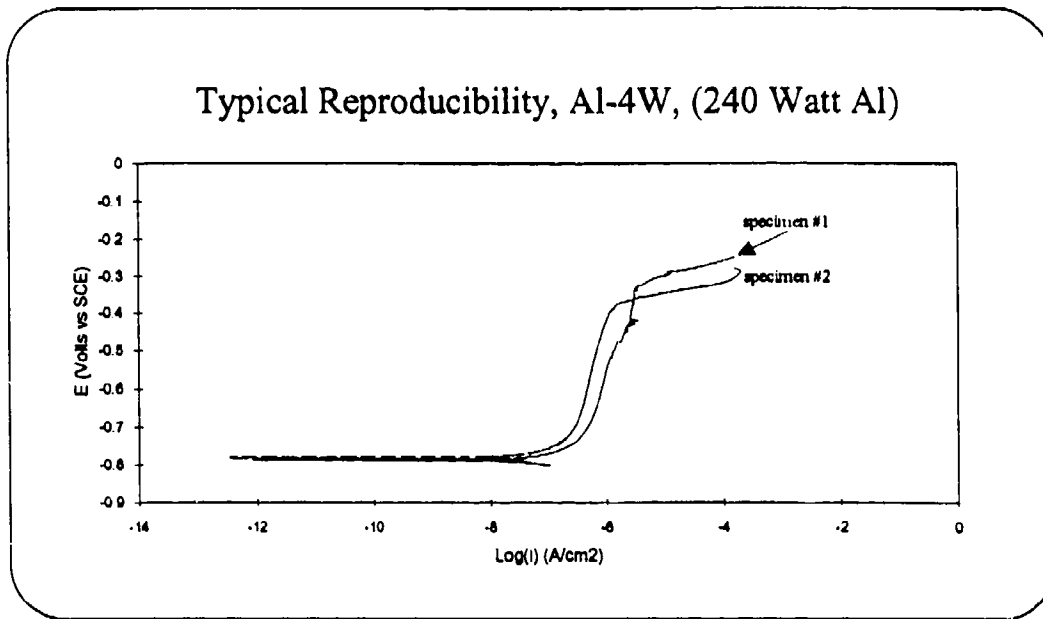


Figure 35. Duplicate Polarization Scans of Al - 4%W,
Representing Typical Reproducibility of the Tests.

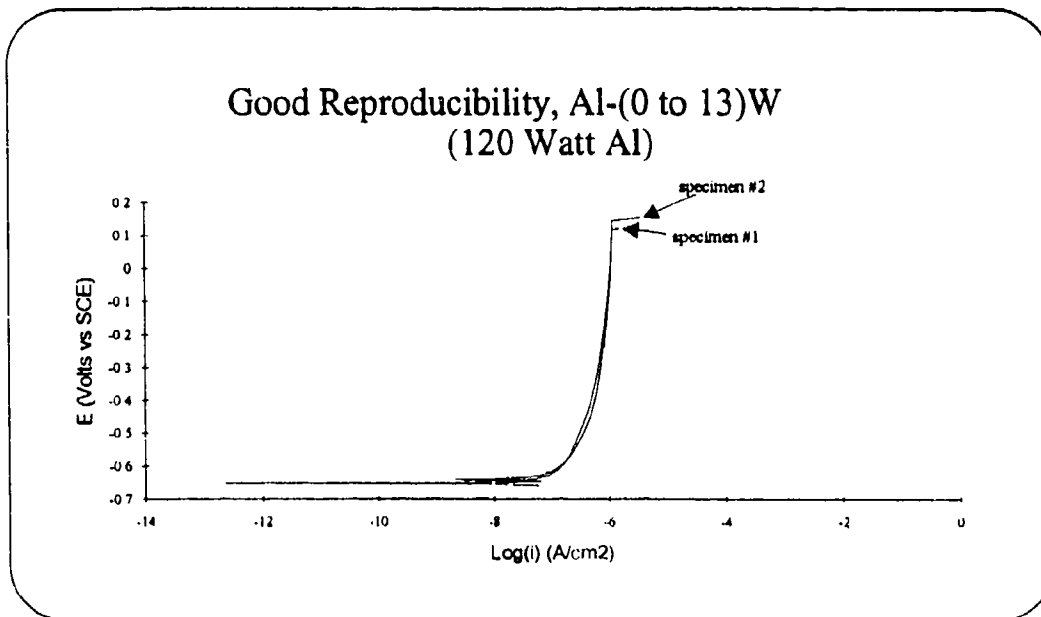


Figure 36. Duplicate Polarization Scans of Al - (0 to 13%)W,
Representing Good Reproducible Curves.

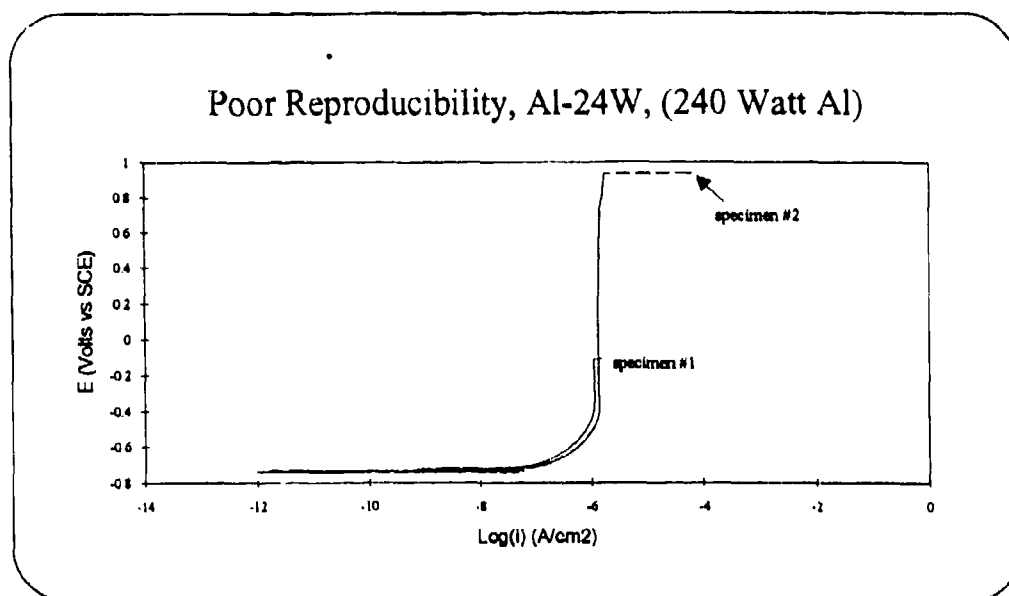


Figure 37. Duplicate Polarization Scans of Al-24W, Representing Very Poor Reproducible Curves.

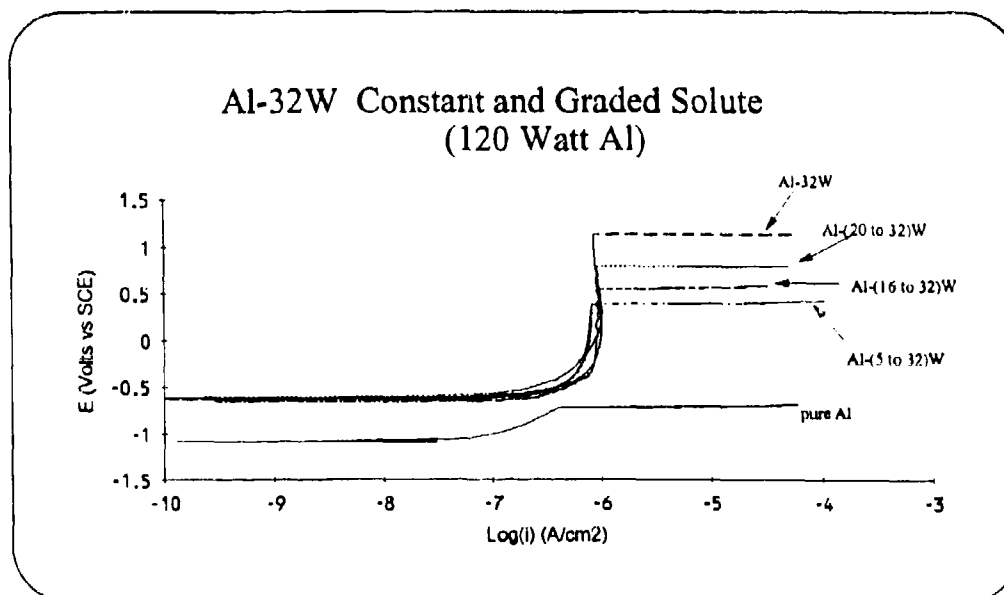


Figure 38. Al-32W Constant and Graded Solute (120 Watt Al), 0.1MNaCl, pH=8.0, quiescent.

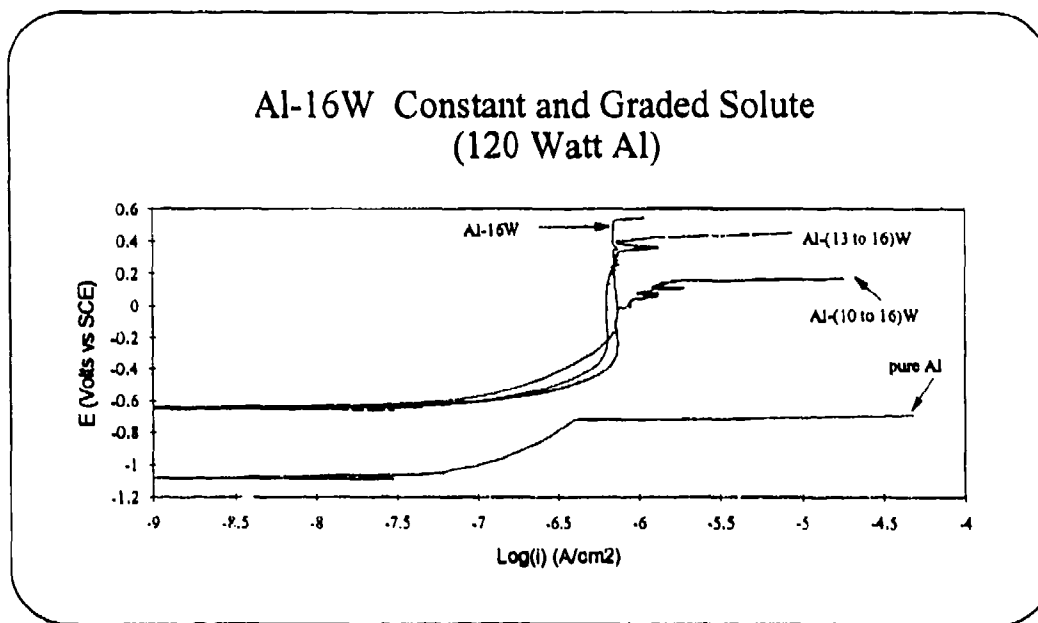


Figure 39. Al-16W Constant and Graded Solute (120 Watt Al),
0.1MNaCl, pH=8.0, quiescent.

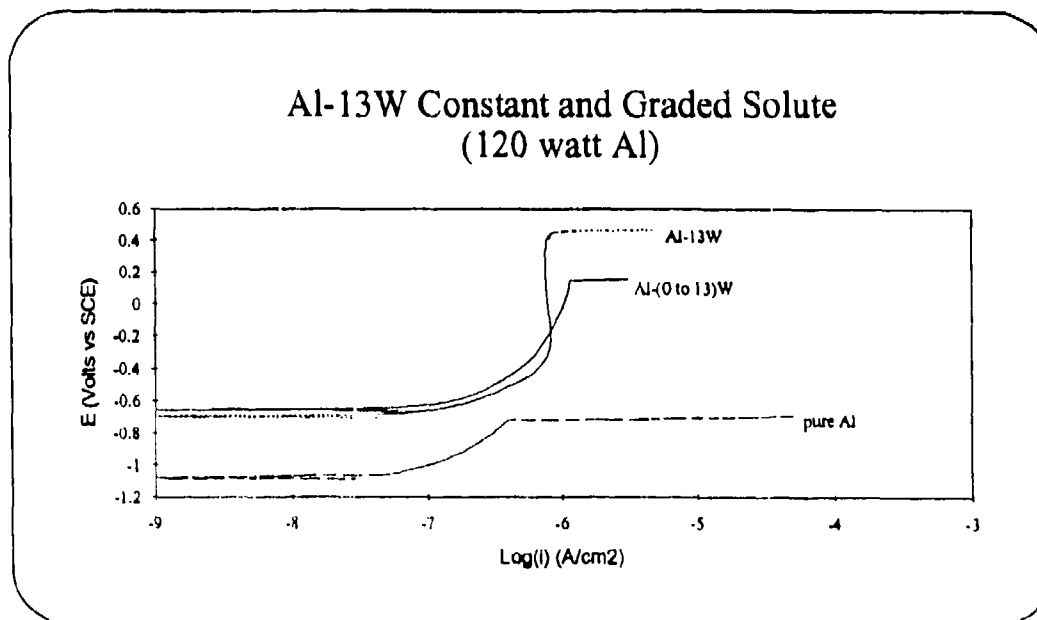


Figure 40. Al-13W Constant and Graded Solute (120 Watt Al),
0.1MNaCl, pH=8.0, quiescent.

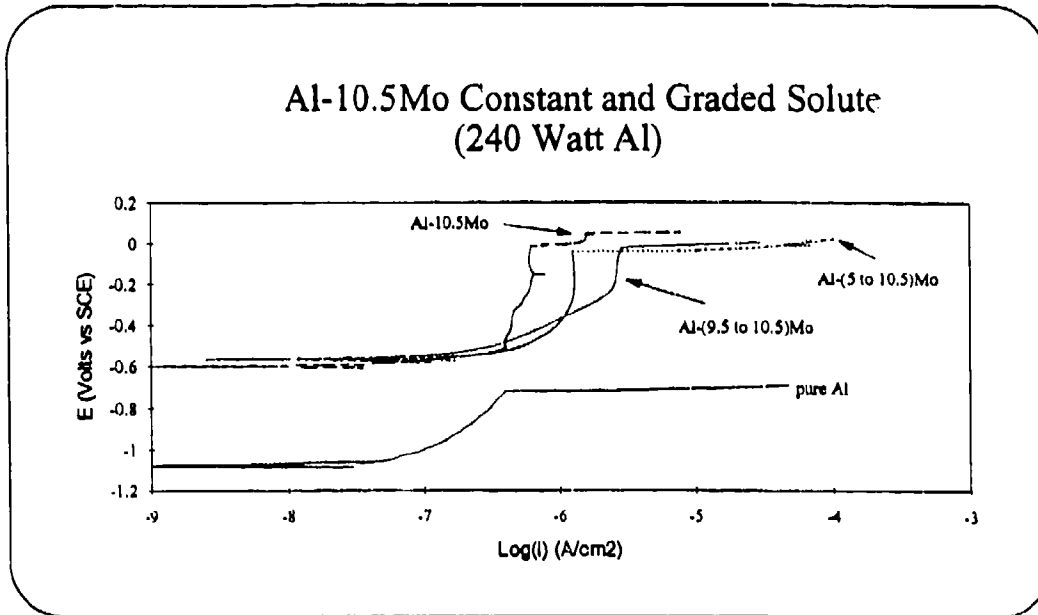


Figure 41. Al-10.5Mo Constant and Graded Solute (240 Watt Al),
0.1MNaCl, pH=8.0, quiescent.

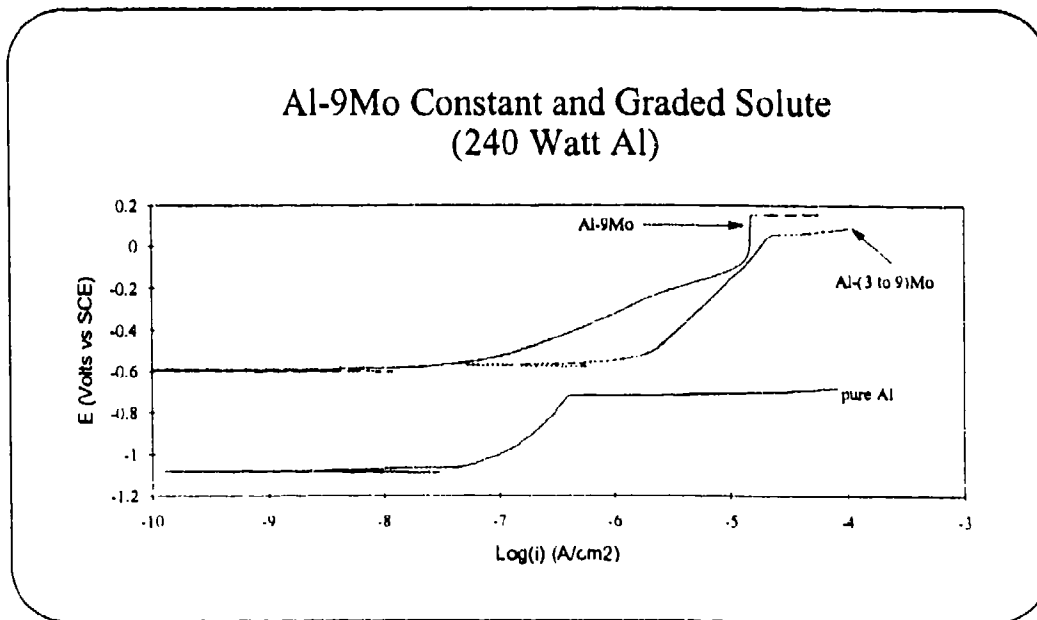


Figure 42. Al-9Mo Constant and Graded Solute (240 Watt Al),
0.1MNaCl, pH=8.0, quiescent.

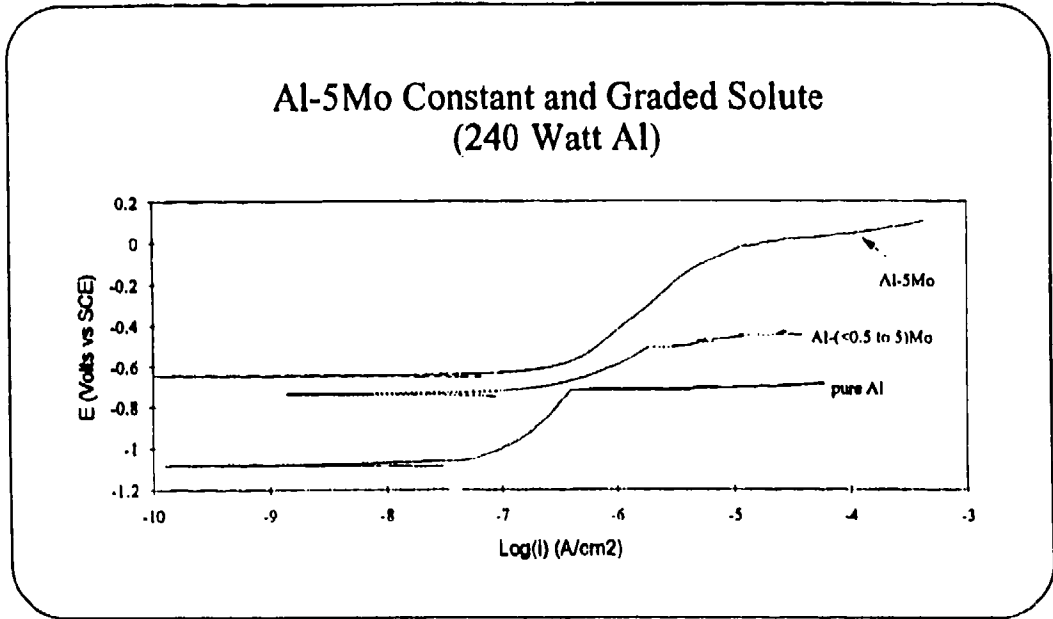


Figure 43. Al-5Mo Constant and Graded Solute (240 Watt Al), 0.1MNaCl, pH=8.0, quiescent.

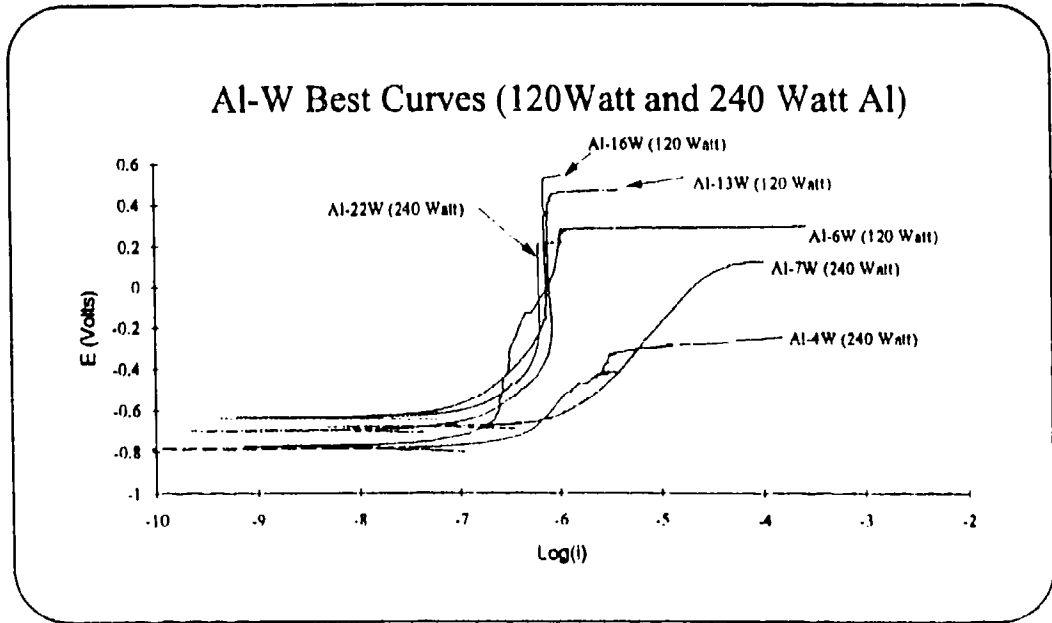


Figure 44. Al-W Polarization Curves Fabricated with either 120 Watt or 240 Watt Al Target Power.

REPORT DOCUMENTATION PAGE

Form Approved
OMB No. 0704-0188

1a. REPORT SECURITY CLASSIFICATION Unclassified		1b. RESTRICTIVE MARKINGS None	
2a. SECURITY CLASSIFICATION AUTHORITY		3. DISTRIBUTION/AVAILABILITY OF REPORT Unrestricted	
2b. DECLASSIFICATION/DOWNGRADING SCHEDULE			
4. PERFORMING ORGANIZATION REPORT NUMBER(S)		5. MONITORING ORGANIZATION REPORT NUMBER(S)	
6a. NAME OF PERFORMING ORGANIZATION Penn State University	6b. OFFICE SYMBOL (if applicable) Code	7a. NAME OF MONITORING ORGANIZATION	
6c. ADDRESS (City, State, and ZIP Code) Dept. of Engineering Science and Mechanics 227 Hammond Bldg. University Park, PA 16802		7b. ADDRESS (City, State, and ZIP Code)	
8a. NAME OF FUNDING/SPONSORING ORGANIZATION Office of Naval Research	8b. OFFICE SYMBOL (if applicable) Code 3312	9. PROCUREMENT INSTRUMENT IDENTIFICATION NUMBER	
6c. ADDRESS (City, State, and ZIP Code) 800 North Quincy St. Arlington, VA 22217-5000		10. SOURCE OF FUNDING NUMBERS	
		PROGRAM ELEMENT NO.	PROJECT NO. N00014- 93-1-0537
		TASK NO.	WORK UNIT ACCESSION NO.
11. TITLE (Include Security Classification) Enhancement of Corrosion Resistance and Mechanical Properties of Light-Weight Metals Through the use of Graded Nonequilibrium Microstructures			
12. PERSONAL AUTHOR(S) B.A. Shaw and K.A. Kennedy			
13a. TYPE OF REPORT Technical	13b. TIME COVERED FROM 7/1/93 TO 6/30/94	14. DATE OF REPORT (Year, Month, Day) 94/10/15	15. PAGE COUNT 60
16. SUPPLEMENTARY NOTATION			
17. COSATI CODES		18. SUBJECT TERMS (Continue on reverse if necessary and identify by block number)	
FIELD	GROUP	SUB-GROUP	Functionally graded materials, nonequilibrium alloying, corrosion resistant Al alloys, corrosion resistant Mg alloys
19. ABSTRACT (Continue on reverse if necessary and identify by block number)			
<p>Designs for the future will place extreme demands on light-weight materials. In order to meet the challenges of the future it is vital that an emphasis be placed on tailor-making these materials to enhance specific properties. Through the use of rapid solidification processing advances have been made in our ability to engineer materials, but we have yet to be able to tailor-make a light-weight alloy with all of the characteristics we desire. A new approach to tailor-making alloys with the enhanced properties we desire is to use nonequilibrium alloying techniques such as sputter or high-rate vapor deposition to grade the structure and composition of an alloy during processing. Such alloys could be designed to take advantage of recent advances in enhancing both the mechanical properties and the corrosion resistance of Al and Mg. For conventional Al alloys, a combination of high strength and significantly enhanced corrosion resistance are mutually exclusive. In order to achieve high strengths, precipitates are necessary in the microstructure. On</p> <p style="text-align: right;">(continued on back)</p>			
20. DISTRIBUTION/AVAILABILITY OF ABSTRACT <input checked="" type="checkbox"/> UNCLASSIFIED/UNLIMITED <input type="checkbox"/> SAME AS RPT. <input type="checkbox"/> DTIC USERS		21. ABSTRACT SECURITY CLASSIFICATION	
22a. NAME OF RESPONSIBLE INDIVIDUAL B.A. Shaw		22b. TELEPHONE (Include Area Code) (814) 865-7828	22c. OFFICE SYMBOL

19. Abstract (continued)

the other hand in order to exhibit good corrosion performance, a one phase structure is usually required (precipitates can establish microgalvanic cells which lead to accelerated corrosion of the precipitate or the alloy adjacent to the precipitate). Both of these properties could be combined in one material, however, if the structure and composition of the alloy were graded during nonequilibrium processing of the alloys. Work during the first year of this investigation has focused on an evaluation of the morphology and residual stresses present in sputter-deposited Al-Mo and Al-W alloys (both constant and graded compositions) and their influence on alloy corrosion resistance. Results from this investigation reveal that it is possible to produce graded alloys with significantly enhanced corrosion resistance. The level of enhancement is dependent upon the initial solute concentration in graded alloys and the morphology of the sputtered alloy. The most important factor governing corrosion resistance of the alloys is morphology of the deposit, with the densest structures yielding the best corrosion performance.